

AN ABSTRACT OF THE PROJECT OF

Nicholas C. Brown for the degree of Master of Science in Civil Engineering presented on 08 December 2010.

Title: Experiments on the Accuracy of a 3D Motion Capture System

Abstract approved:

---

Merrick C. Haller

Motion capture is the process of recording the movement of objects in three dimensional space over time. Manufacturers design motion capture systems for animation applications and do not provide accuracy information suitable for research. The project goal was to quantify the accuracy of the Phase Space Impulse<sup>®</sup> motion capture system as it is used in the Hinsdale Wave Research Laboratory. Static measurements were evaluated by measuring a known distance between two rigid bodies. Dynamic measurements were evaluated by recording the motion of a pendulum simultaneously with the Phase Space Impulse<sup>®</sup> motion capture system and with an optical encoder. It was shown that the location of a rigid body measured by the motion capture system can be expected to be within 4.1 mm of its actual location, regardless of velocity. Repeated measurements of the same position will have a precision of at least 0.8 mm.

©Copyright by Nicholas C. Brown

08 December 2010

All Rights Reserved

Experiments on the Accuracy of a 3D Motion Capture System

by  
Nicholas C. Brown

A PROJECT REPORT

submitted to

Oregon State University

in partial fulfillment of  
the requirements for the  
degree of

Master of Science

Presented December 08, 2010  
Commencement: June 2011

Master of Science project report of Nicholas C. Brown presented on December 08, 2010.

APPROVED:

---

Major Professor, School of Civil and Construction Engineering

---

Head of the School of Civil and Construction Engineering

---

Dean of the Graduate School

I understand that my project report will become part of the permanent collection of Oregon State University libraries. My signature below authorizes release of my project report to any reader upon request.

---

Nicholas C. Brown, Author

## ACKNOWLEDGEMENTS

The author expresses sincere appreciation to David Newborn. David's motivation to create a survivable motion capture system is a great benefit to the O.H. Hinsdale Wave Laboratory. Without the development of his epoxy waterproofing method the need for this project would not have existed. David introduced the author to the accuracy problem, demonstrated the ins, outs and quirks of the PhaseSpace system and provided much needed guidance in electronics and data acquisition. Most importantly, David's work ethic and commitment to the field of Ocean Engineering are truly inspiring.

The author would also like to thank his advisor, Dr. Merrick Haller, for providing hours of guidance throughout his graduate studies. Dr. Haller was always available to render assistance with a wide array of topics, from linear wave theory to rigid body kinematics. His calm demeanor, clear communication and desire to teach helped to make the authors pursuit of a Master of Science degree a pleasant endeavor.

Finally, the author would like to thank his academic peers, Jeff Travis, David Honegger, Kerri Bridges, Jeff Oskamp, Tuk Jitraporn, Kelley Ruehl, Steve Meicke and Justin Hovland for their shared wisdom, assistance, and most importantly, friendship.

## TABLE OF CONTENTS

	<u>Page</u>
1 Introduction.....	1
2 Literature Review.....	2
3 Methods and Materials.....	3
3.1 The PhaseSpace System.....	3
3.1.1 Calibration.....	5
3.1.2 Origin and Axis Selection.....	8
3.1.3 Motion Capture.....	9
3.1.4 Waterproofing Active Impulse <sup>®</sup> LEDs.....	10
3.2 Static Test Procedure.....	12
3.3 Dynamic Test Procedure.....	14
4 Results.....	20
4.1 Static Test Results.....	19
4.1.1 Known Distance Between Rigid Bodies.....	20
4.1.2 PhaseSpace Distance Between Rigid Bodies...	20
4.2 Dynamic Test Results.....	26
4.2.1 Optical Encoder Signal.....	27
4.2.2 Rotating and Translating the Optical Encoder signal	29
4.2.3 Identifying and Accounting for a Phase Shift..	33
4.2.4 Dynamic Error Calculation.....	34
5 Discussion.....	43
5.1 Static Test Discussion.....	43
5.1.1 Accuracy and Precision Dependency on..... Location	43
5.1.2 Accuracy and Precision Dependency on the.... Length of Calibration	44

## TABLE OF CONTENTS (Continued)

	<u>Page</u>
5.1.3 Accuracy and Precision Dependency on the.... Length of Calibration	45
5.2 Dynamic Test Discussion.....	45
5.2.1 Error in the Encoder Signal.....	46
5.2.2 Pendulum Movement Outside of x"-y' Plane ' .	47
5.2.3 Accuracy and Precision Dependency on..... Velocity	48
5.2.4 Accuracy Dependency on Pendulum ..... Amplitude	48
6 Conclusion .....	49
6.1 Static Accuracy and Precision.....	49
6.1.1 Location in the Measurement Field .....	49
6.1.2 Calibration Length .....	50
6.1.3 Epoxy Encapsulation .....	50
6.1.4 Accuracy and Precision Under Wave Lab..... Conditions	50
6.2 Dynamic Accuracy.....	51
6.3 Future Work .....	52
6.4 Final Conclusions.....	53
Bibliography .....	54
Appendices.....	55
Appendix A: Trial Two Dynamic Figures.....	56
Appendix B: Trial Three Dynamic Figures .....	59
Appendix C: Trial Four Dynamic Figures .....	62

## LIST OF FIGURES

<u>Figure</u>	<u>Page</u>
1. Speed Rail <sup>®</sup> frame and Impulse <sup>®</sup> cameras .....	3
2. Setup of PhaseSpace components .....	4
3. Euler Converter output.....	5
4. Calibration Wand .....	5
5. Calibration data displayed in the measurement field.....	7
6. Axis alignment square.....	8
7. Carbon fiber rod.....	9
8. LED Mold .....	11
9. LED before and after epoxy encasement.....	11
10. Static apparatus .....	12
11. Static apparatus at the second highest elevation .....	13
12. Different static test elevations.....	14
13. Dynamic apparatus; front view .....	15
14. Dynamic apparatus; view from below .....	15
15. LEDs mounted to the pendulum .....	17
16. $l$ , $w$ and $\theta$ measurements on the dynamic apparatus .....	17
17. Dynamic apparatus data acquisition schematic .....	18
18. Example of converging length measurement between rigid..... bodies.	21
19. Example of typical length measurement between rigid..... bodies over time.	21

## LIST OF FIGURES (Continued)

<u>Figure</u>	<u>Page</u>
20. Example of a False Rapid Change in Length Between ..... Rigid Bodies	22
21. Precision and accuracy results; eight minute calibration ..... and epoxy encased LEDs	24
22. Precision and accuracy results; eight minute calibration ..... and exposed LEDs	24
23. Precision and accuracy results; four minute calibration ..... and epoxy encased LEDs	25
24. Precision and accuracy results; four minute calibration ..... and exposed LEDs	25
25. Filtered and unfiltered encoder as a function of time .....	27
26. Detailed view of the encoder angle signal .....	28
27. Determining PhaseSpace start time in encoder signal .....	28
28. Dynamic apparatus geometry .....	30
29. Pendulum reference frame translation and rotations .....	31
30. Identifying time lag in encoder signal .....	34
31. x position signals and accuracy vs. time .....	35
32. y position signals and accuracy vs. time .....	36
33. z position signals and accuracy vs. time .....	37
34. Calculated velocity and accuracy vs. time .....	39
35. Position error as a function of velocity, first trial .....	40
36. Position error as a function of velocity, second trial .....	42
37. Position error as a function of velocity, third trial .....	41

LIST OF FIGURES (Continued)

<u>Figure</u>	<u>Page</u>
38. Position error as a function of velocity, forth trial .....	42
39. Accuracy and time as functions of velocity .....	42
40. Encoder error vs. PhaseSpace error; x signal, first peak.....	46
41. Encoder error vs. PhaseSpace error; x signal, last peak .....	47
42. Pendulum motion outside of x"-y" plane .....	48

## LIST OF TABLES

<u>Table</u>	<u>Page</u>
1. Static analysis summary.....	26
2. Component and total signal accuracy and standard deviation, first trial.....	38
3. PhaseSpace error mean and standard deviation for ..... all trials	43

## Experiments on the Accuracy of a 3D Motion Capture System

### 1. Introduction

The motion of floating objects are of importance to engineers and scientists in a range of applications. For example, in the design of ships and wave energy convertors and the study of debris mobilized by tsunamis. Measuring the movement of floating objects in the laboratory can be challenging. Six degrees of freedom are required to capture the full range of motion; three translational and three rotational. Onboard systems such as gyroscopes often cannot be included without altering the movement of the object.

Motion capture systems provide a relatively non-intrusive method to quantify the movement of a floating object and record the data digitally. They were originally developed as a tool to record the movement of actors for the generation of computer generated imagery. Manufacturers still design the systems for animation applications. However, accuracy information suitable for experimentation and research has not been determined by manufacturers (DeLuzio et al. 1993).

The O.H. Hinsdale Wave Research Laboratory at Oregon State University operates a Phase Space Impulse<sup>®</sup> motion capture system. The system is configured with a measuring field of 6m x 6m in length and width and up to 6m in height, which is suitable for use over portions of the 104m x 3.7m Large Wave Flume or the 48.8m x 26.5m Tsunami Wave Basin. In order to validate motion measurements of objects in the flume or the tsunami basin the accuracy of the Phase Space Impulse<sup>®</sup> system must be determined.

The project goal is to quantify the accuracy and precision of position measurements using the Phase Space Impulse<sup>®</sup> motion capture system and to determine if these measurements are affected by a protective epoxy encapsulation, calibration, location in the measurement field or rigid body velocity.

## 2 Literature Review

Three journal articles were reviewed to discover what other types of motion capture systems are available, if they have been tested for accuracy and if so, by what means. These are Castro et al. (2005), Teeple et al. (2009), and ReinFrank et al. (2010)

The intent of Castro et al. (2005) was to develop a low cost motion capture system that used video and then determine its accuracy. One unique advantage of the author's system (SOMCAD3D) was that it provided motion capture without the use of markers on the object being tracked. The motion capture system required 6.3 minutes of post processing time to obtain three dimensional position measurements from two dimensional images. Accuracy was evaluated by placing at known distances from each other in the measurement field and then measuring the distance between the markers with the motion capture system. The mean length error was found to be 2.48 mm with a standard deviation of 2.12 mm.

Teeple et al (2009) also evaluated the accuracy of several motion capture systems that used video. Five different systems were evaluated. The study was of particular interest because it introduced the use of a pendulum to provide known movement to evaluate the performance of the motion capture systems. The pendulum apparatus consisted of a 4.3 kg, 0.36 m long cylinder that would swing freely with a natural frequency of 0.872 Hz. The position of the pendulum in time was modeled using an equation for simple harmonic motion. The five motion capture systems all provided angular position accuracy of 3–5% and angular speed accuracy of 5–15% compared to motion as predicted by the simple harmonic motion equation.

In the proceedings of OMAE 2010 a paper was presented on the testing of wave energy devices in the O.H. Hinsdale Wave Laboratory (Rhinefrank, et al. 2010) In it, the Phase Space Impulse<sup>®</sup> Motion Capture system was introduced as a commercial system that can be used to track object motion in a wave tank. The authors show that the accuracy of a target's position measurement depends on the distance the target is from the center of the measurement field. Accuracy was evaluated by measuring the distance

between two LEDs with a rotary XY table and with the motion capture system. Measurements were repeated at different distances from the center of the measurement field. Accuracy was found to be 1.3 mm within a 2.5 m radius, improving to 0.9 mm within a 1.2 m radius.

### 3 Methods and Materials

#### 3.1 The PhaseSpace System

The Phase Space Impulse<sup>®</sup> motion capture system (henceforth referred to simply as PhaseSpace) is a commercial product used in the O.H. Hinsdale Wave Laboratory. It consists of eight Impulse<sup>®</sup> cameras, a server, 90 active Impulse<sup>®</sup> LEDs, a dedicated laptop computer, an LED base station, LED controllers, a calibration wand, an alignment axis square, a Speed-Rail<sup>®</sup> frame and carbon fiber poles.

The eight Impulse cameras<sup>®</sup> are mounted on the Speed-Rail<sup>®</sup> frame and aimed at a location in the center of the desired measurement field. CAT 5E Ethernet cable is used to provide a connection between the cameras and the server computer. USB cables are



Figure 1: Speed Rail<sup>®</sup> frame and Impulse<sup>®</sup> cameras.

used to connect the LED base station (located on top of the server) and the LED controllers to the server while the laptop computer is connected with ethernet cable. Figures 1 and 2 show the Speed-Rail<sup>®</sup> frame setup used in this experiment.

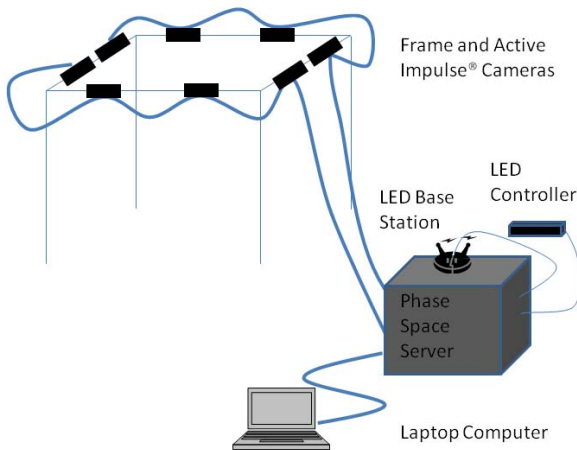


Figure 2: Setup of PhaseSpace components.

The laptop computer is equipped with four programs to manage the motion capture process. A configuration manager, accessed through the laptop web browser, allows the user to program LED controllers. A calibration manager provides an interface for the calibration process and a master program provides an interface for the actual motion capture. Finally, a Euler converter program converts the motion data into more useful Euler coordinates of three translational components ( $x$ ,  $y$  and  $z$ ) and three rotational components (roll, pitch and yaw). Figure 3 illustrates the information obtained from the Euler converter program.

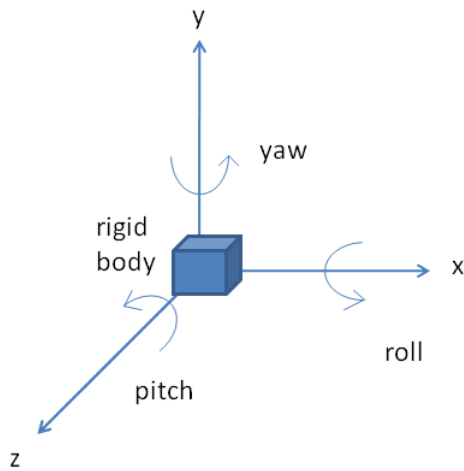


Figure 3: Euler Converter output.

### 3.1.1 Calibration

Before any motion capture data can be collected, the system must be calibrated. This is done using a rigid shaft or "wand" consisting of eight LEDs mounted at known locations along the wand. The operator uses the configuration manager to encode a LED controller with a calibration profile. This profile consists of a numbered identity for each LED on the wand. The geometry of the LED locations relative to one another are known in the server's software. The LED controller is then disconnected from the server and connected to the wand. The operator opens the calibration program and connects the motion capture system. Figure 4 shows the calibration wand.



Figure 4: Calibration wand.

Anytime the PhaseSpace system is "connected" the base station wirelessly commands the LED controller to turn on the LEDs. The controller specifies which LEDs turn on and provides power to the LEDs. The LEDs flash at specific frequencies unique to their numbered identity. Each of the eight Impulse<sup>®</sup> cameras use two linear detectors working in stereo to detect the direction, distance and identity of the LEDs in the measurement field. This information is collected by the server computer at 480 Hz.

Next, an operator selects "capture" from the calibration manager and begins to move the calibration wand throughout the measurement field. PhaseSpace records the movement of each LED as the operator moves the wand so that calibration data are collected evenly throughout the entire measurement field. As a visual aid, the calibration manager displays eight squares, each divided into nine equal components. The squares represent the field of view of each camera. When sufficient data are collected in each region of a camera's field of view the corresponding component square is turned green. This lets the user know when sufficient data have been collected throughout the measurement field.

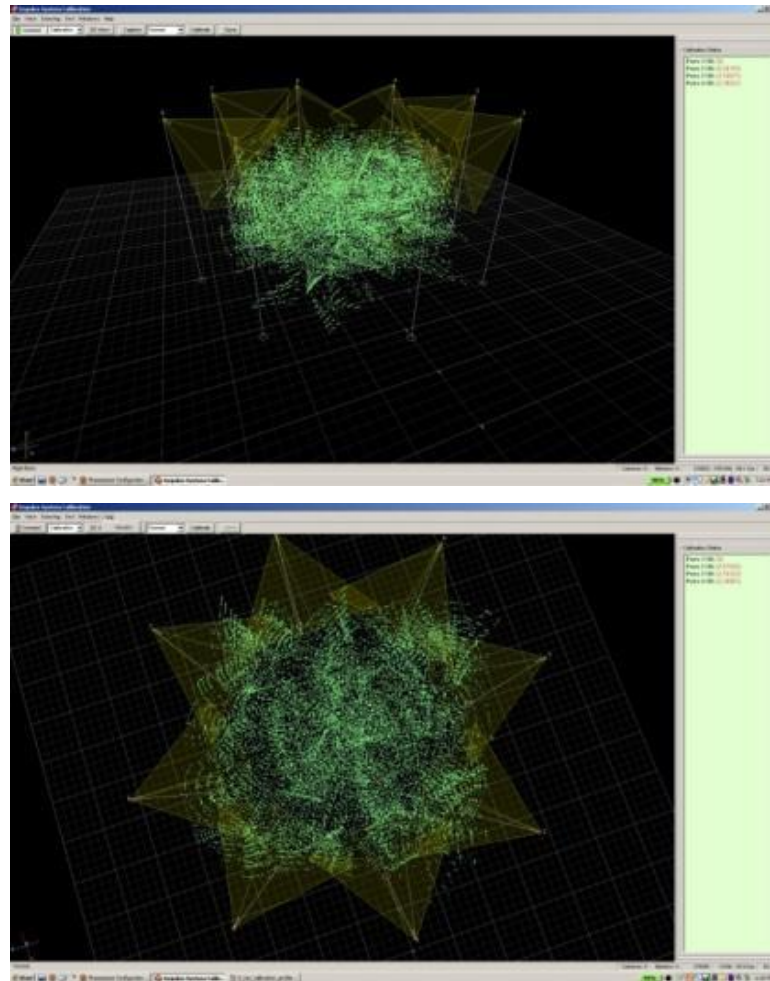


Figure 5: Calibration data displayed in the measurement field.

Once sufficient data have been collected, the operator clicks "calibrate" and then "disconnect" to turn off the LEDs. When the server computer has finished its calibration calculations, the calibration manager notifies the operator. The operator clicks "save" and the calibration process is completed. Figure 5 shows the display from the calibration manager after the calibration process has been completed. The above image shows a perspective view of the measurement field, and below image shows a view from above. The yellow cones represent the cameras' fields of view, and the white lines represent the cameras' positions projected onto the x-z horizontal plane.

### 3.1.2 Origin and Axis Selection

The next step in the motion capture process is to specify an inertial coordinate system comprised of an origin and three axes in the measurement field. The operator removes the LED controller from the calibration wand and connects it to the server using a USB cable. The configuration manager is used to encode a new LED profile for the axis alignment square on the LED controller. The controller is then removed from the computer server and attached to the axis alignment square.

The alignment axis square consists of three LEDs placed so that they represent the corners of a right triangle. The LED which is at the intersection of the legs of the right triangle acts as the origin, and the other two identify the "x" and "z" axes. The plate is placed in the measurement field at the desired location for the origin and leveled using two bubble levels attached to the plate. The "y" axis extends from the origin LED upwards and normal to the plane described by the other LEDs. Figure 6 shows the alignment axis square.

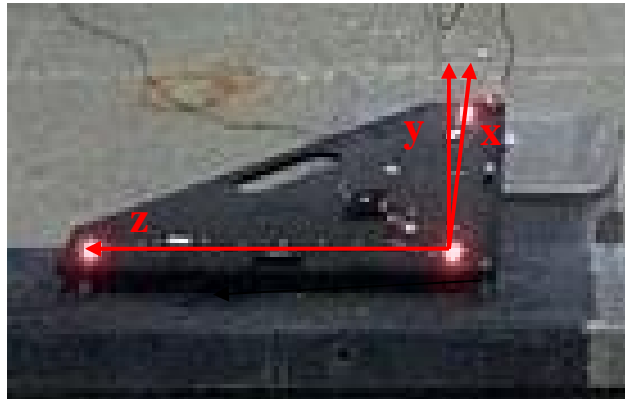


Figure 6:Alignment axis.

The calibration manager is opened again and "align" is selected instead of "calibrate" The operator then selects "connect", illuminating the LEDs on the alignment

square, and the origin and three axes are specified for the motion capture system when the operator selects "save".

### *3.1.3 Motion Capture*

Three non-collinear LEDs are required to define a rigid body's orientation in space (DeLuzio et al. 1993). For the PhaseSpace system in the O.H. Hinsdale Wave Lab sets of three LEDs are mounted to rigid carbon fiber rods at varying angles of orientation. This allows markers to be quickly attached to a rigid body at a single point. Additionally, the rods keep LEDs above the surface when rigid bodies rest low in the water. Figure 7 shows a carbon fiber rod.



Figure 7: Carbon fiber rod.

To manage and organize the LEDs in the measurement field, the Configuration Manager is used to generate and encode specific profiles on LED controllers. Each LED controller can manage up to 72 LEDs. More than three LEDs, or multiple carbon fiber poles can be used to identify a single rigid body. Multiple rigid bodies can be connected to the same LED controller.

Once the PhaseSpace system has been calibrated, the origin and axes have been defined, LEDs on carbon fiber poles have been attached to rigid bodies, and LED controllers have been encoded and attached to the LEDs the motion capture process is ready to begin. The operator opens the Master program and connects the system. This

turns on the Impulse<sup>®</sup> cameras and the LED base station wirelessly commands the LED controller to turn on the LEDs

The operator uses the Master program to compile the LEDs into groups for each rigid body. The groups are then saved as a file type unique to PhaseSpace (.rb). Individual LEDs flash at unique frequencies so that they can be identified by the cameras. LEDs are assigned a number by the manufacturer based on this identity. The location of the rigid body is defined as the location of the LED with the lowest numbered identity. This location is given as the distance from the origin in the three directions defined by the inertial coordinate system so that the rigid body has an x, y and z coordinate. A body frame of reference is assigned to each rigid body so that the initial orientation of the rigid body matches the orientation of the inertial axis defined by the axis alignment square. To initiate motion capture, the operator selects "record" and the PhaseSpace system records the location and orientation of each rigid body at 480 Hz. When the desired motion has completed, the operator selects "stop" and saves the captured motion information to another file type unique to PhaseSpace (.rpd).

The Euler converter program can then be used to generate Microsoft Excel .csv files from the .rpd and .rb files. The .csv file contains nine columns, six of which represent the three translational coordinates and three rotational coordinates for each of the samples recorded by the PhaseSpace system. Two additional columns provide the sample number and a confidence interval for each measurement. The confidence interval is negative when the PhaseSpace system cannot resolve the location of a rigid body.

#### *3.1.4 Waterproofing Active Impulse<sup>®</sup> LEDs*

Several expensive components of the PhaseSpace system are placed at risk if installed on floating bodies under wave action. Water exposure and impact shock could potentially damage or destroy LEDs. To increase their survivability, Mr. David Newborn has encased LEDs in an optically transparent three part epoxy resin. Figure 8 is an image of the epoxy molds and Figure 9 shows the LEDs before and after encasement. The

accuracy and precision provided by Reinfrank et al. (2010) was determined using exposed LEDs. The effect of the epoxy encasement on the accuracy of the PhaseSpace system was one of the primary motivations for this project.

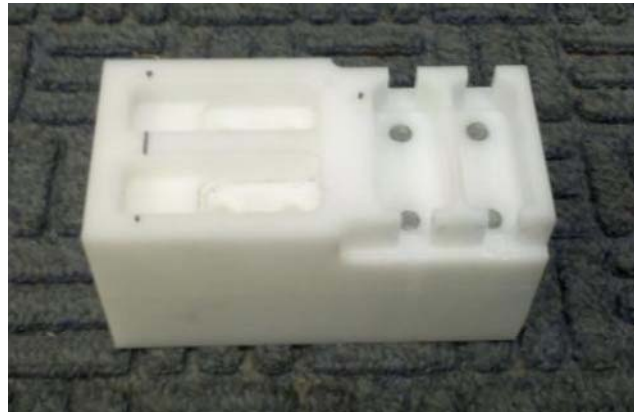


Figure 8: LED mold.

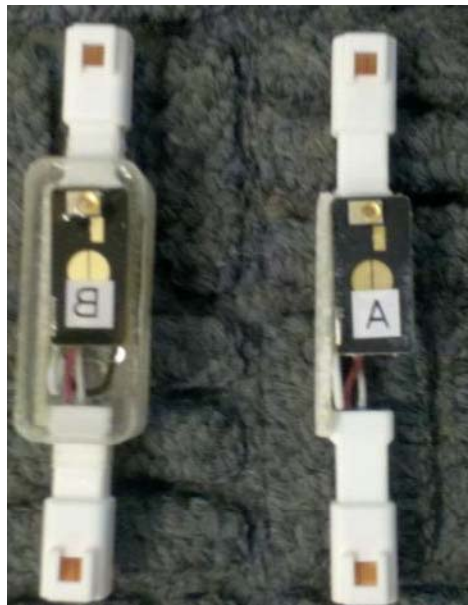


Figure 9: LED before and after epoxy encasement. The before LED is on the right.

### 3.2 Static Test Procedure

To evaluate accuracy, the distance between two rigid bodies would be calculated from PhaseSpace location data and compared to the "true" distance measured by hand. An apparatus was constructed to allow the distance between two rigid bodies to be held consistent throughout the experiment. Four LED poles were attached at known distances along a thin but inflexible wood board. Each rigid body would consist of two poles separated by 38 cm. This setup would mimic the spacing of poles on model wave energy buoys currently being tested at the O.H. Hinsdale wave lab. Three epoxy encased LEDs and three exposed LEDs were attached to each pole. The center poles which contained the LEDs defining the position of the rigid bodies, were spaced approximately 13 cm and were joined by a piece of plastic to ensure the distance between rigid bodies remained consistent. Figure 10 shows the static apparatus.

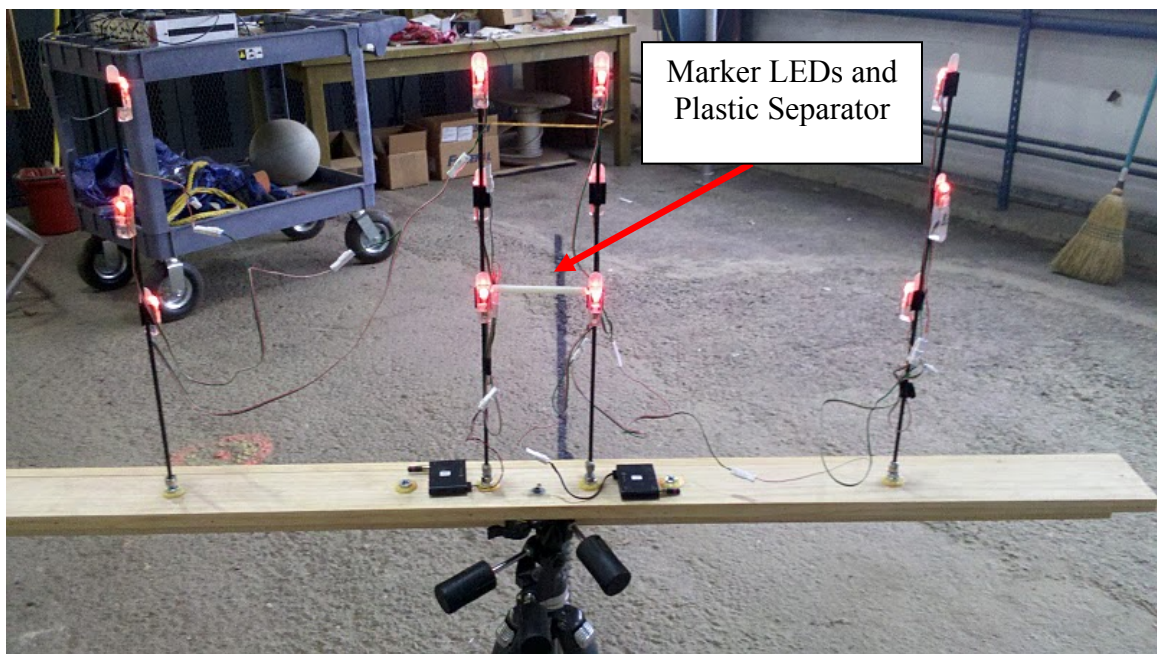


Figure 10: Static apparatus.

In Figure 10, the LEDs marking the location of the rigid bodies can be identified by the white piece of delrin. Measurements of the distance between the center of the LEDs defining the location of each rigid body were taken by hand with calipers that provide accuracy to a thousandth of an inch. This measurement was repeated eight times for both the exposed and epoxy encased LEDs.

Measurement locations were marked on the floor of the measurement field using spray paint. The center of the field was chosen as a measurement location, and five other locations were marked at 60 centimeter intervals in a line extending from the center towards the perimeter of the measurement field. Measurements would be taken at each location at five different heights by placing the rigid body apparatus on the floor or mounted on a tripod set to four different elevations. Figures 11 and 12 show the static apparatus in the center of the measurement field at one of the five heights.



Figure 4: Static apparatus at the second highest elevation. The line marks additional horizontal measurement locations.



Figure 5: Different static test elevations.

A calibration was performed for a duration of approximately eight minutes. At each of the thirty locations defined by the five locations and four heights motion capture data was collected for approximately 30 seconds with the epoxy encased LEDs. This process was repeated using the exposed LEDs. Finally, the entire process was repeated for epoxy and exposed LEDs with a calibration of four minutes.

### 3.3 Dynamic Test Procedure

The second part of this project was to determine the accuracy of the PhaseSpace system in determining the location of a moving rigid body with the epoxy encased LEDs. It was of particular interest to determine if accuracy was substantially different than seen in the static analysis and to determine if accuracy changes with velocity. In this test the swinging motion of rigid body mounted to a pendulum would be measured with an optical encoder while being recorded by the PhaseSpace system. The motion capture data would then be compared to the optical encoder data to determine accuracy. The components of the apparatus used for dynamic testing are shown in Figures 13 and 14.

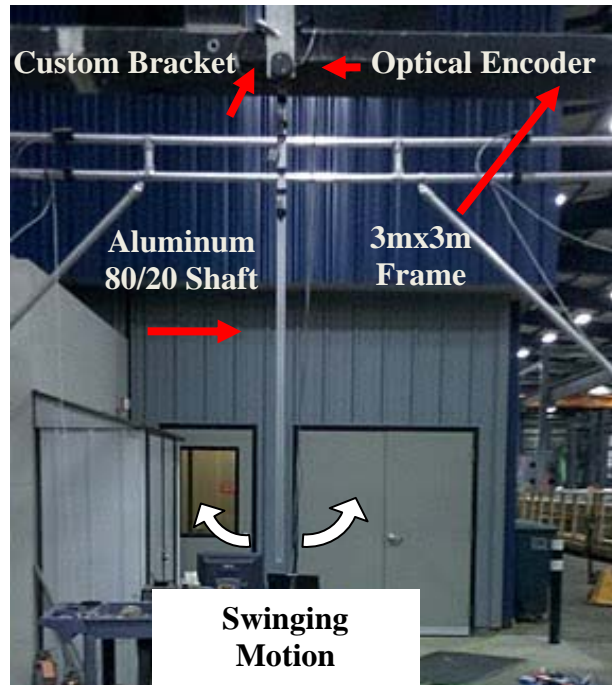


Figure 6: Dynamic apparatus; front view.

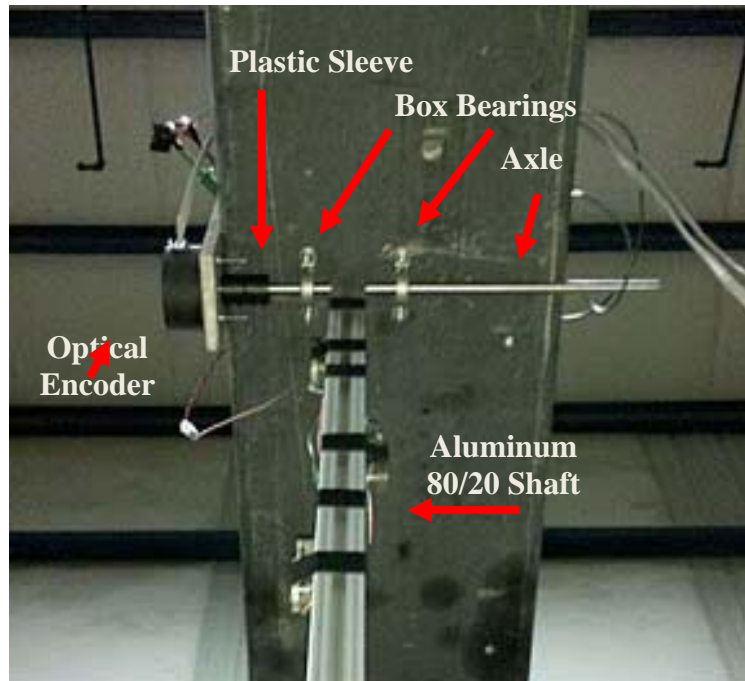


Figure 7: Dynamic apparatus; view from below.

A large three meter by three meter aluminum frame was placed in the center of the measurement field. An axle was created using an aluminum cylinder that passed through two box bearings attached to the frame. A US Digital A2 optical encoder was attached to one end of the axle with a plastic sleeve and mounted to the frame with a custom bracket. An aluminum 80/20 shaft was machined so that it could slide over and attach to the axle set screw. The axle and 80/20 shaft could swing freely in the box bearings while the optical encoder provided angle measurements with an advertised accuracy of 0.18 degrees (0.0031 radians).

Before attaching the 80/20 shaft to the axle three epoxy encased LEDs were mounted to the shaft using electrical tape with a spacing mimicking that of the carbon fiber poles. The top and bottom LEDs were mounted on the same face of the 80/20 shaft while the middle LED was mounted on the opposite side. A rotary XY table was used to determine the distance between the LED and the center of the axle in a plane perpendicular to the axle. This distance is termed  $l$ . Another measurement, termed  $w$ , describes the distance the top LED rests from the centerline of the 80/20 shaft in the same plane used to measure  $l$ . Figure 15 shows the LEDs on the shaft and Figure 16 illustrates the two length measurements and the angle measured by the encoder, labeled  $\theta$ .

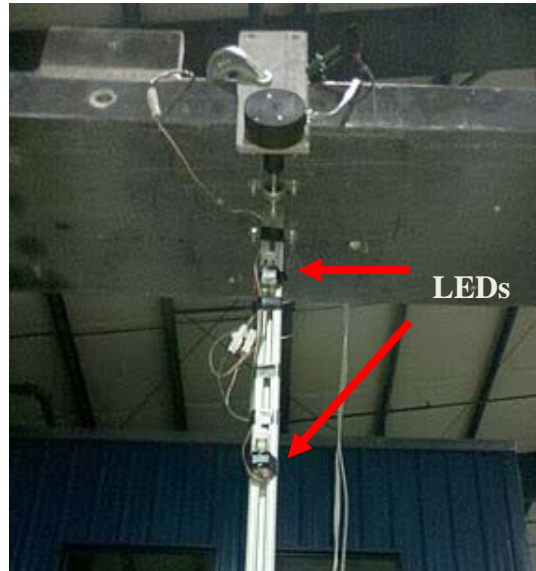


Figure 8: LEDs mounted to the pendulum.

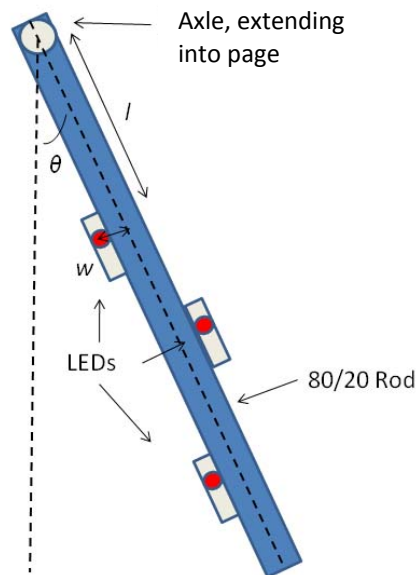


Figure 9:  $l$ ,  $w$  and  $\theta$  Measurements on the dynamic apparatus.

Data acquisition for the second part of the experiment was managed on the laptop. The optical encoder signal ran through a RJ25 phone cable. The encoder power and the accompanying ground leg of the cable were connected to a 6.5 volt power supply. The signal leg and its ground were connected to channel one of an analog filter. After passing through the filter, the encoder signal was sent to an Analog/Digital (A/D) converter board. Figure 17 is a schematic of the dynamic apparatus power and signal connections.

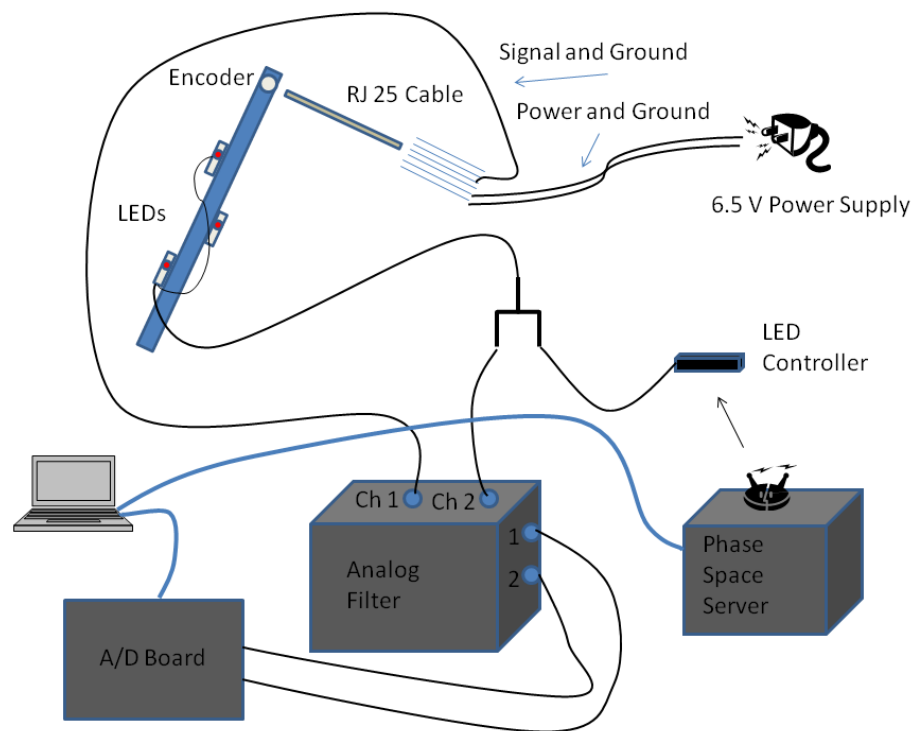


Figure 17: Dynamic apparatus data acquisition schematic.

User inputs to the PhaseSpace system start at the laptop computer. The laptop computer was connected to the PhaseSpace server by an Ethernet cable. The LED base station, connected to the server with a USB cable, communicated wirelessly with the LED controller. The LED controller signal was split in parallel and passed to both the second analog filter channel and to the LEDs. After passing through channel two, the

LED controller signal was passed through the A/D board and ultimately to the laptop computer.

To prepare for motion capture, an eight minute calibration was performed and the alignment square was placed in the measurement field so that the 80/20 shaft was approximately over the origin and the x-axis was approximately aligned with the plane that the shaft would swing through once displaced.

The motion capture process began with the LED controller signal disconnected from the splitter that sent the signal in parallel to the LEDs and the analog filter. The TracerDAQ program was set to record the two channels at 480Hz for 30 seconds. The operator first connected the PhaseSpace system. Next, the "record" button in the TracerDAQ program was pressed so that the program began recording both channels. The operator would then walk over to the cable that was disconnected from the LED controller splitter and connect it. The operator would immediately displace the shaft by hand, release it and let it swing freely. After TracerDAQ finished recording 30 seconds the PhaseSpace system would be disconnected using the Master program. Three additional trials were performed using the same calibration data.

## 4 Results

### 4.1 Static Test Results

During the static test procedure the PhaseSpace system produces location information, consisting of three translational coordinates for the two rigid bodies, for 30 second intervals at 480 Hz. Measurements were taken at thirty locations throughout the measurement field under four different conditions (eight minute calibration with epoxy encased LEDs, eight minute calibration with exposed LEDs, four minute calibration with epoxy encased LEDs and four minute calibration with exposed LEDs). The accuracy of the PhaseSpace system was evaluated by calculating the distance between rigid bodies for the thirty second intervals and comparing it to a known length measured by hand. The

precision of the PhaseSpace system was determined by evaluating the spread of the measurements at each location.

#### 4.1.1 Known Distance Between Rigid Bodies

The true distance between rigid bodies was estimated using the eight measurements taken by hand. A "Student's T" distribution was used to determine a 95% confidence interval for the true length:

$$95\% CI = \bar{x} \pm t \frac{s}{\sqrt{n}}$$

Where  $\bar{x}$  is the mean of the sample distribution of eight measurements,  $s$  is the sample standard deviation  $t$  is a constant defined by the size and shape of the distribution and  $n$  is the number of samples. The 95% confidence interval for the epoxy encased LEDs was found to be  $129.95 \pm 0.08$  mm and the 95% confidence interval for the exposed LEDs was found to be  $92.73 \pm 0.06$  mm.

#### 4.1.2 PhaseSpace Distance Between Rigid Bodies

For each of the thirty specified locations throughout the measurement field, PhaseSpace collected thirty seconds of position data for the rigid bodies at 480Hz. The distance between rigid bodies was calculated using a root-sum-square equation for the entire thirty second series:

$$d = \sqrt{(x_{rb1} - x_{rb2})^2 + (y_{rb1} - y_{rb2})^2 + (z_{rb1} - z_{rb2})^2}$$

where  $d$  is the distance between rigid bodies and  $x$ ,  $y$  and  $z$  are the three translational coordinates provided by PhaseSpace for each rigid body.

It quickly became apparent that the first five seconds of capture data was not accurate. When calculated length was plotted against time, the length seemed to converge on a final value over the first five seconds. Figure 18 shows an example of this convergence.

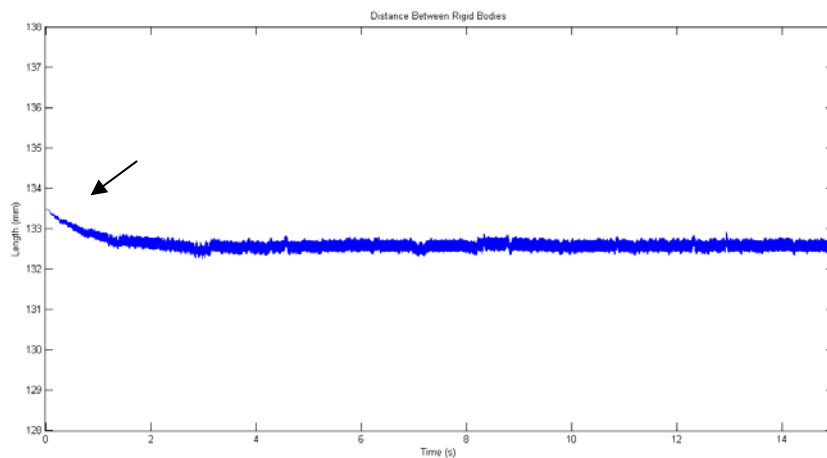


Figure 18: Example of converging length measurement between rigid bodies.

Because of this feature, length data was only selected from five seconds until thirty seconds. Figure 19 is an example of a typical measured length plotted over time for any given location.

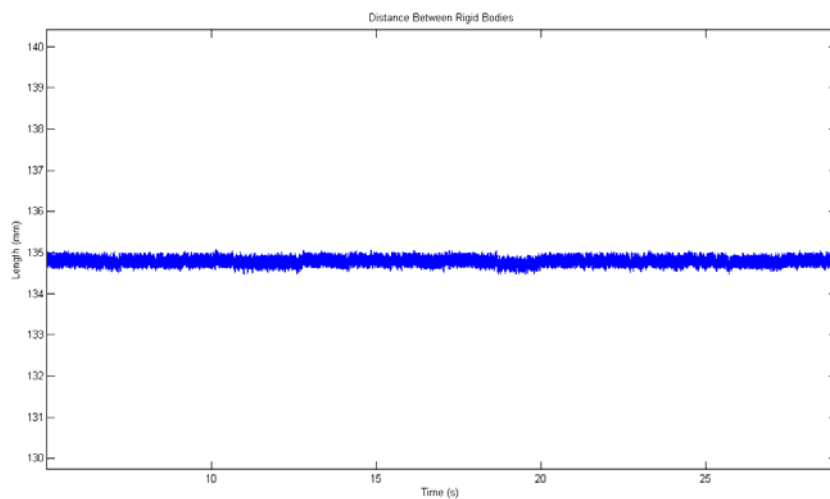


Figure 19: Example of typical length between rigid bodies over time.

Measurements at some locations showed evidence that PhaseSpace would falsely recorded a rapid change in the distance between rigid bodies. An example of this is Figure 20.

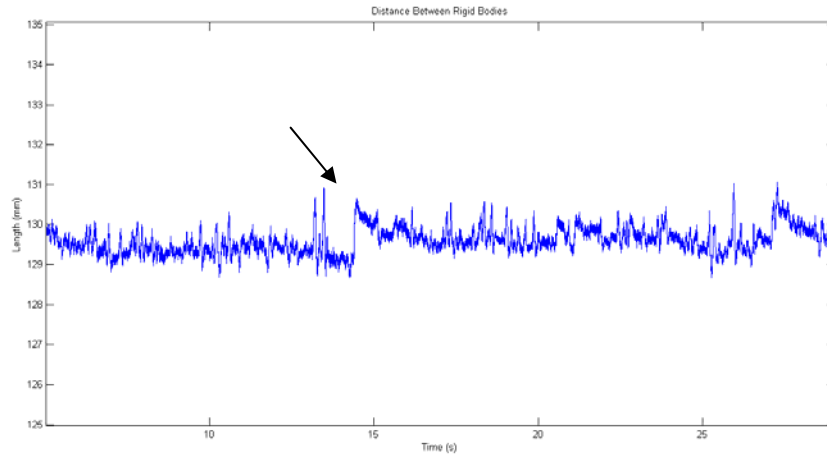


Figure 10: Example of a false rapid change in length between rigid bodies

At each of the thirty measurement locations, the mean length and the standard deviation of all lengths was calculated for the 25 second intervals. A 99.7% confidence interval ( $\pm$  three standard deviations) was used to determine the precision of the measurements recorded during the 25 seconds. The accuracy (or error) of the measurements was determined by subtracting the known length between rigid bodies from the mean length calculated by PhaseSpace.

Figures 21 through 24 show the accuracy and precision values plotted as a function of radial position in the measurement field for the four evaluated conditions. Each 25 second measurement is represented by a colored square. The x axis represents the distance of each measurement location from the center of the measurement field in the horizontal, or x-z, plane. The y axis represents the height in the measurement field of each measurement location. The color of each square represents the precision or accuracy of the 25 second measurement. In each case smaller values correspond with

greater accuracy (less error) or precision (smaller confidence interval). The elevation of the cameras is marked with a solid line and the elevation of the center of measurement field is marked with a dashed line.

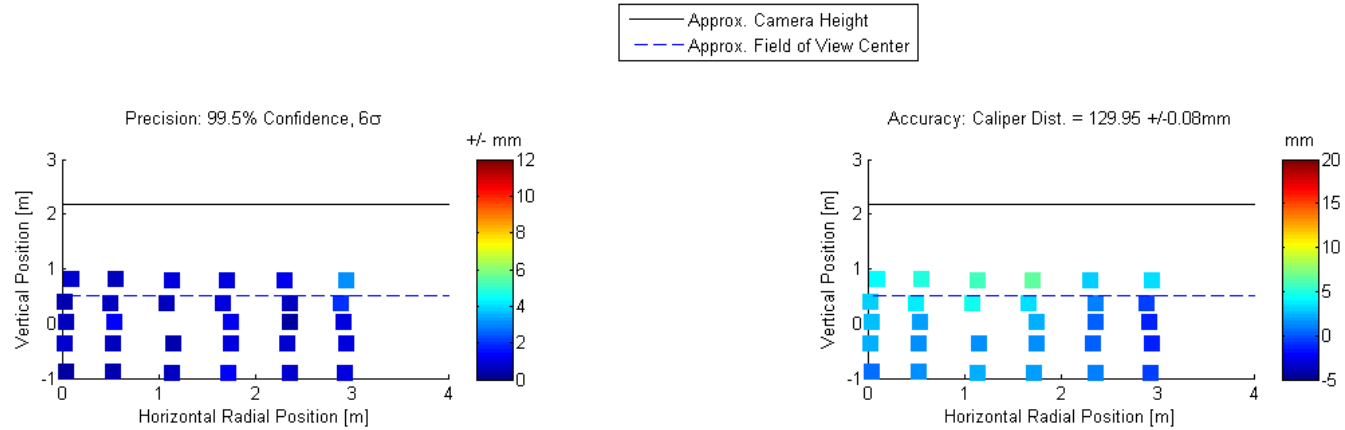


Figure 11: Precision and accuracy results; eight minute calibration and epoxy encased LEDs.

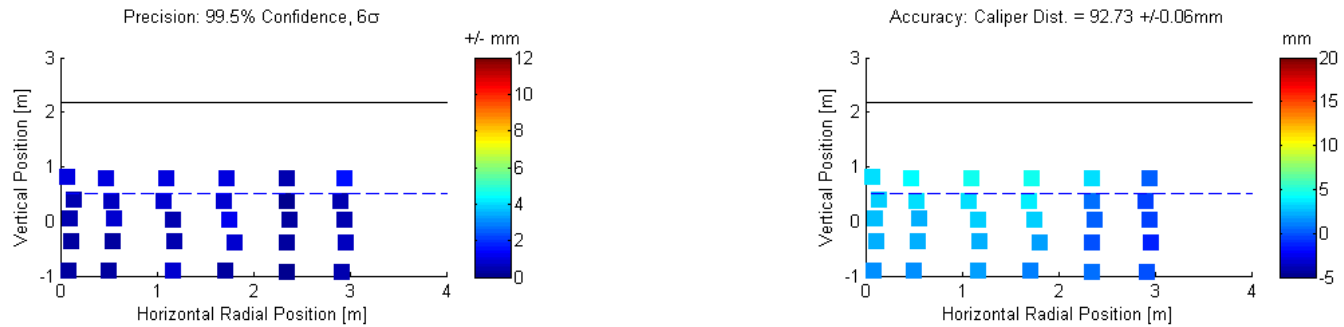


Figure 12: Precision and accuracy results; eight minute calibration and exposed LEDs.

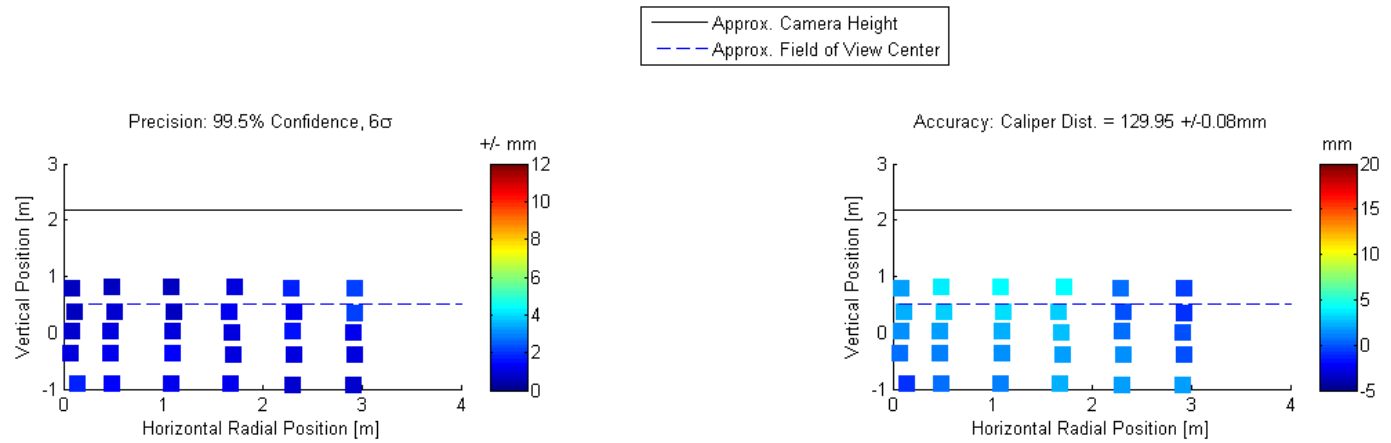


Figure 13: Precision and accuracy results; four minute calibration and epoxy encased LEDs.

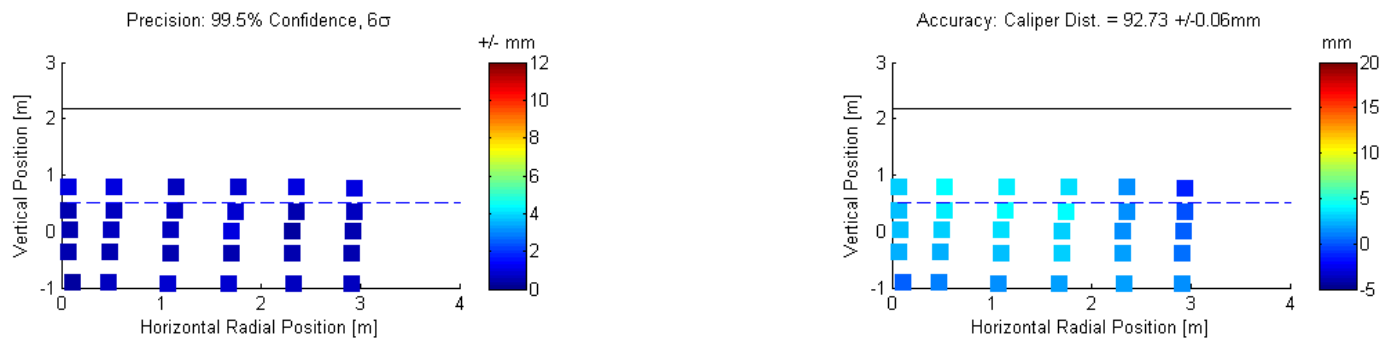


Figure 14: Precision and accuracy results; four minute calibration and exposed LEDs.

Table 1 summarizes the figures. It provides the mean and standard deviation of the accuracy and precision for populations that include all thirty locations evaluated for the four sets of conditions.

Table 1: Static analysis summary.

	8 Minute Calibration		4 Minute Calibration	
	Epoxy LEDs	Exposed LEDs	Epoxy LEDs	Exposed LEDs
<b>Mean Accuracy</b>	<b>2.11 mm</b>	<b>1.95 mm</b>	<b>1.54 mm</b>	<b>2.18 mm</b>
S.D. Accuracy	1.97	1.61	1.40	1.37
<b>Mean Precision</b>	<b>0.94</b>	<b>0.61</b>	<b>1.15</b>	<b>0.65</b>
S.D. Precision	0.56	0.35	0.42	0.22

## 4.2 Dynamic Test Results

The dynamic test procedure created two files used to evaluate the accuracy and precision of the PhaseSpace system. One was a txt file produced by the TracerDAQ program which contained channel one from the DAQ, the optical encoder angle signal, and channel two from the DAQ, the PhaseSpace signal being sent to the LEDs. These signals were both recorded at 480 Hz. The encoder angle signal, paired with the two lengths taken from the dynamic apparatus geometry, was used to derive the position of the LED marking the rigid body in three dimensional coordinates based on the PhaseSpace origin and axis. A .csv file was provided by the PhaseSpace system that contained the rigid body position and orientation data; also collected at 480 Hz. The distance between the location provided by the optical encoder and the location provided by PhaseSpace at each sample time was used to evaluate the accuracy and precision of the PhaseSpace system.

#### 4.2.1 Optical Encoder Signal

The output signal of the optical encoder was the angle of the shaft measured in volts. The voltage for the series was converted to radians using a conversion factor, provided by the manufacturer, of 3.599 volts per radian. The signal was calibrated so that the rest angle of the apparatus was equal to zero by taking the mean angle measurement while the shaft was at rest (the first second of the signal) and subtracting this value from the entire angle measurement series. To remove noise, a zero-phase filter was applied to the signal using Matlab's *filtfilt* command. This filter avoids a phase shift by processing the input signal in both the forward and backwards directions. Figure 25 shows the entire filtered and unfiltered encoder angle signal while Figure 26 provides a more detailed view of the first peak.

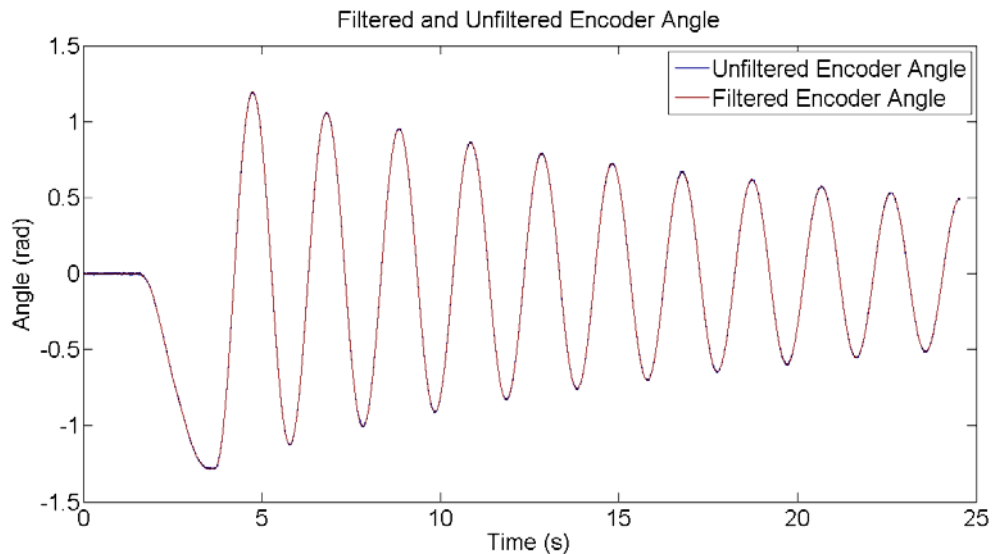


Figure 15: Filtered and unfiltered encoder as a function of time.

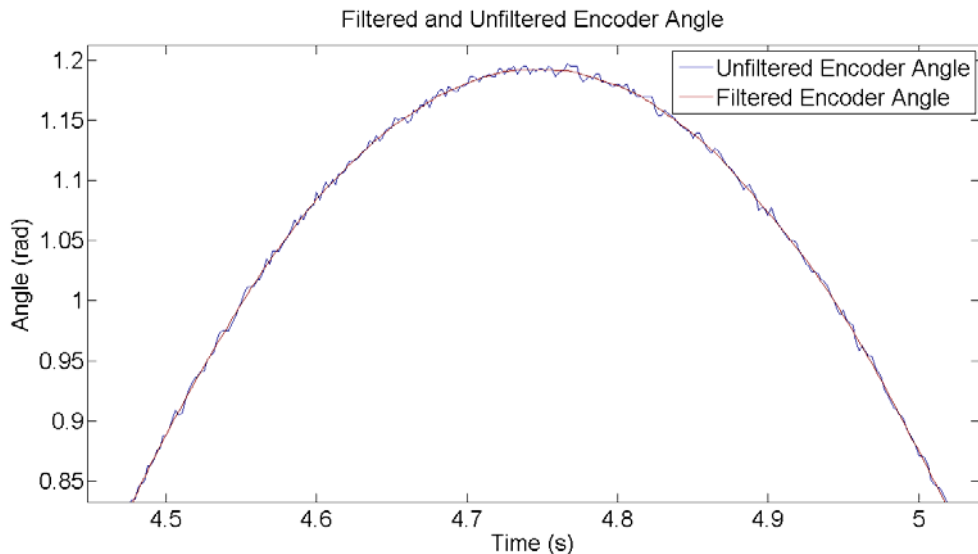


Figure 16: Detailed view of the encoder angle signal.

Because the PhaseSpace system and the laptop computer began recording at separate times during the dynamic accuracy test the two signals are not synchronized in time. Synchronization was accomplished using channel two from the analog filter. Figure 27 shows channel two from the analog filter plotted over time.

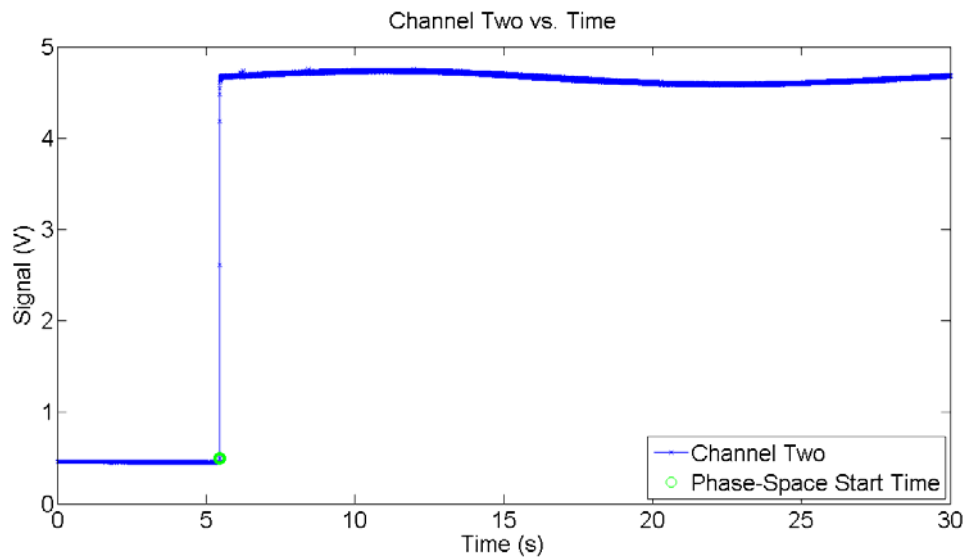


Figure 27: Determining PhaseSpace start time in encoder signal.

In Figure 27, each sample in the signal is plotted with a blue x. At the moment the LED controller connection is made by the operator the signal from channel two jumps from 0.5 volts to over four volts. The time corresponding to the first point in the signal to be more than 1.05 times greater than the mean of channel two for the first tenth of a second is identified. This sample marks the time that the PhaseSpace signal starts in the optical encoder time signal and is identified by a green circle in Figure 27. To synchronize the two signals, this time length is subtracted from the optical encoder time series. Because the laptop computer was measuring both channels at 480 Hz there could still be a 1/480th of a second difference between the time signals of both series.

#### *4.2.2 Rotating and Translating the Optical Encoder Signal*

The encoder angle signal and the two length measurements taken from the aluminum 80/20 shaft,  $l$  and  $w$ , were used to create two dimensional position coordinates in the plane of the pendulum. Figure 28 shows this plane. The  $y''$  axis in the figure represents the line made by the 80/20 shaft when it is at rest. The  $x''$  axis represents the direction normal to the axle of the apparatus when the shaft is at rest. The  $x''$ - $y''$  plane intersects the center of the LED marking the position of the rigid body, which is also the origin of the coordinate system.

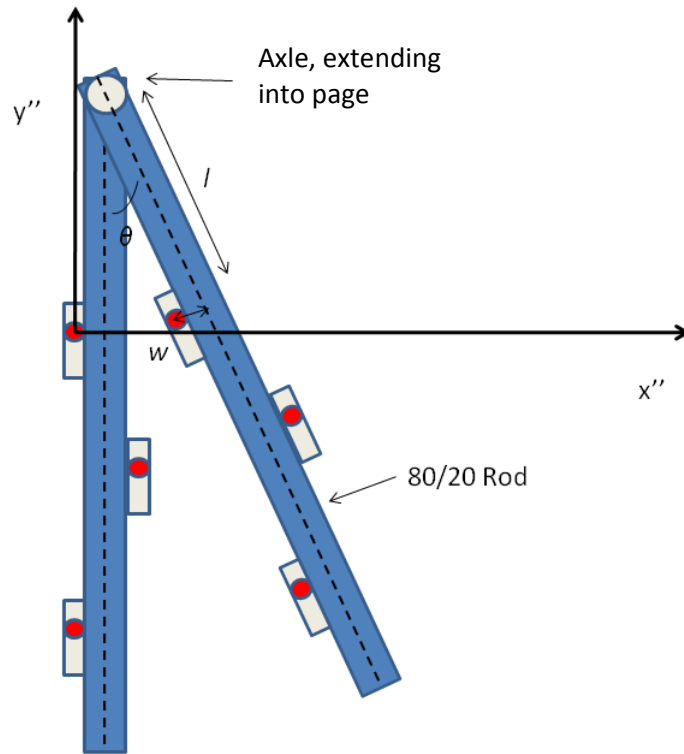


Figure 28: Dynamic apparatus geometry.

This is the reference frame of the pendulum. In this reference frame the position vector of the LED can be written as the sum of the position vector of the center of the axle and the position vector from the center of the axle to the center of the LED:

$$\vec{r}_{LED}(x'', y'') = \vec{r}_{axle} + \vec{r}_{axle-LED}$$

$$\vec{r}_{LED}(x'', y'') = (w\hat{x}'' + l\hat{y}'') + (l\sin(\theta)\hat{x}'' - w\cos(\theta)\hat{x}'' - l\cos(\theta)\hat{y}'' - w\sin(\theta)\hat{y}'')$$

$$\vec{r}_{LED}(x'', y'') = (w + l\sin(\theta) - w\cos(\theta))\hat{x}'' + (l - l\cos(\theta) - w\sin(\theta))\hat{y}''$$

Where  $\theta$  is the encoder angle,  $l$  is the distance from center of the axis to the center of the LED and  $w$  is the distance from the center of the LED to the center of the 80/20 shaft.

The encoder signal is described in only two dimensions. Movement in a third direction would be caused by a "wobble" of the swinging shaft resulting from the small

amount of slop in the box bearings and flex of the shaft. This movement was observed in the PhaseSpace signal and will be shown to be very small.

Had the  $x''$ - $y''$  reference frame of the pendulum been aligned perfectly with the  $x$  and  $y$  directions defined during the alignment of the PhaseSpace system, the above calculations would be sufficient to allow comparison between PhaseSpace and optical encoder signals. However, alignment was not perfect and two rotations and a translation must be performed in order to properly align the optical encoder signal with the PhaseSpace reference frame.

The PhaseSpace signal was used to determine the orientation of the pendulum reference frame with respect to the PhaseSpace coordinate system. First the signal was translated. The average PhaseSpace position of the rigid body LED for the first second of the signal was used as the rest position. The vector from the PhaseSpace origin to the rest position was subtracted from the entire PhaseSpace signal, shifting the signal to the origin. In Figure 29, the pendulum reference frame is shown in red. The black arrow represents the vector from the PhaseSpace origin to the LED rest position.

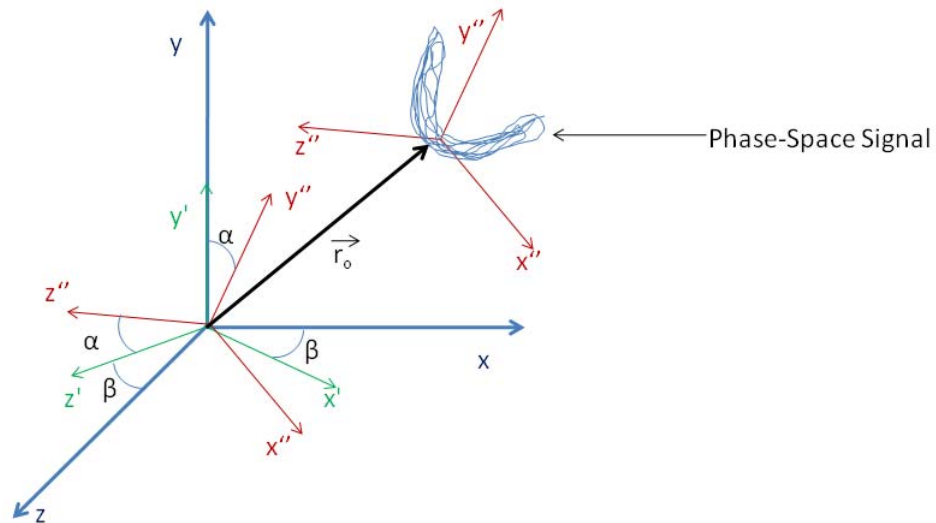


Figure 29: Pendulum reference frame translation and rotations.

The vector for the translated PhaseSpace signal can be written as:

$$\vec{r}_{trans}(x, y, z) = \vec{r}_{LED} - \vec{r}_o$$

where:

$$\vec{r}_{LED}(x, y, z) = x_p\hat{x} + y_p\hat{y} + z_p\hat{z}$$

$$\vec{r}_o(x, y, z) = x_o\hat{x} + y_o\hat{y} + z_o\hat{z}$$

The subscript  $p$  denotes the  $x$ ,  $y$  and  $z$  components of the PhaseSpace signal. The subscript  $o$  denotes the rest position of the LED marking the rigid body with respect to the PhaseSpace coordinate system. Substituting and reorganizing, the equation for the translated signal can be written as:

$$\vec{r}_{trans}(x, y, z) = (x_p - x_o)\hat{x} + (y_p - y_o)\hat{y} + (z_p - z_o)\hat{z}$$

Two rotations were required to align the PhaseSpace and pendulum frames. One rotation,  $\beta$ , was about the  $x$  axis while another,  $\alpha$ , was about the  $y$  axis. The rotation about  $y$  accounts for the plane the pendulum swings through being slightly misaligned with the  $x$  axis of the PhaseSpace reference frame. The rotation about  $x$  accounts for the axle of the pendulum not being perpendicular with the direction of gravity. Because when properly aligned, the shaft swings freely in the  $x$ - $y$  plane, a rotation about  $z$  is not needed. Figure 29 further illustrates the rotation angles.

To find the angles  $\alpha$  and  $\beta$  a least squares regression was used to fit a plane to the entire PhaseSpace signal for the LED marking the rigid body. The equation for the plane was found to be:

$$ax + by + cz = 0$$

$$a = -0.0032 \quad b = -0.0018 \quad c = 1.0$$

with the coefficients of  $a$ ,  $b$  and  $c$  representing the  $x$ ,  $y$  and  $z$  components of the normal vector from the plane.

The angles  $\alpha$  and  $\beta$  can be found as:

$$\alpha = -\tan^{-1}(b/c) = 0.0018 \text{ radians}$$

$$\beta = \tan^{-1}(a/c) = -0.0032 \text{ radians}$$

and are shown in Figure 29.

Angles  $\alpha$  and  $\beta$  will rotate the x-y plane of the PhaseSpace frame to be in line with the x"-y" plane of the dynamic apparatus. To rotate the dynamic apparatus frame to the PhaseSpace frame the negative of angles  $\alpha$  and  $\beta$  should be used. The rotation matrices which will properly rotate the optical encoder signal so that it will overlap the PhaseSpace signal are:

$$R_y = \begin{bmatrix} \cos(-\beta) & 0 & -\sin(-\beta) \\ 0 & 1 & 0 \\ \sin(-\beta) & 0 & \cos(-\beta) \end{bmatrix} \quad R_x = \begin{bmatrix} 1 & 0 & 0 \\ 0 & \cos(-\alpha) & -\sin(-\alpha) \\ 0 & \sin(-\alpha) & \cos(-\alpha) \end{bmatrix}$$

Because the rest position of the pendulum was not at the origin of the inertial frame, it must be translated to properly match the rigid body locations provided by PhaseSpace. The vector used for the translation is the same vector,  $\vec{r}_o$  that was subtracted from the PhaseSpace signal in order to find the angles  $\alpha$  and  $\beta$ . The rotations and translation are represented as:

$$\vec{r}_{enc}(x, y, z) = ([R_y][R_x] * \vec{r}_{x''y''}) + \vec{r}_o$$

where  $\vec{r}_{x''y''}$  is the original position signal found from the optical encoder signal,  $\vec{r}_o$  is the vector from the PhaseSpace origin to the rest position of the rigid body LED and  $\vec{r}_{enc}(x, y, z)$  is the rotated and translated position signal from the optical encoder which can be used with the PhaseSpace signal to determine accuracy.

#### 4.2.3 Identifying and Accounting for a Phase Shift.

Figure 30 is a plot of the x component of the PhaseSpace and optical encoder position signals with time. The axis of the figure were scaled to identify the first peak after the dynamic apparatus had been released and allowed to swing freely.

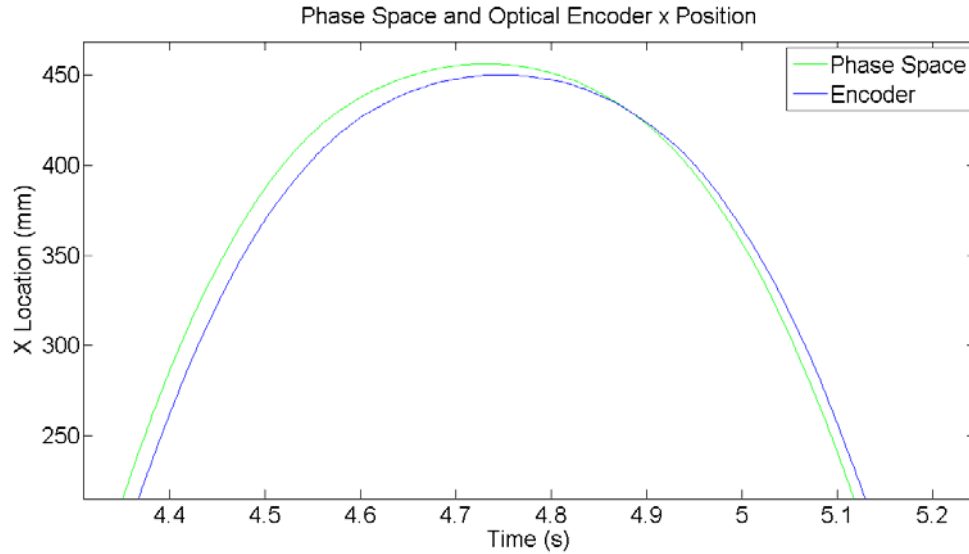


Figure 30: Identifying time lag in encoder signal.

Figure 30 shows that the signal peaks do not occur at the same time. There is a seven sample, 0.0146 second, difference between the two peaks. This difference was observed in each of eleven x peaks in the signals and is larger than the possible 1/480th of a second difference identified during the synchronization of time scales. To account for this the optical encoder signal was shifted forward in time by the seven sample intervals.

#### 4.2.4 Dynamic Error Calculation

Figures 31 through 34 show the PhaseSpace x, y and z signals and the rotated and translated optical encoder x, y and z signals for the first trial. The time lag has been removed. The component accuracy is calculated as the difference between the two signals. The error of the total signal is also presented. This was calculated by taking the root of the sum of the of the differences between the signals in the three directions as shown below:

$$Total\ Error = \sqrt{(x_{p.s.} - x_{o.e.})^2 + (y_{p.s.} - y_{o.e.})^2 + (z_{p.s.} - z_{o.e.})^2}$$

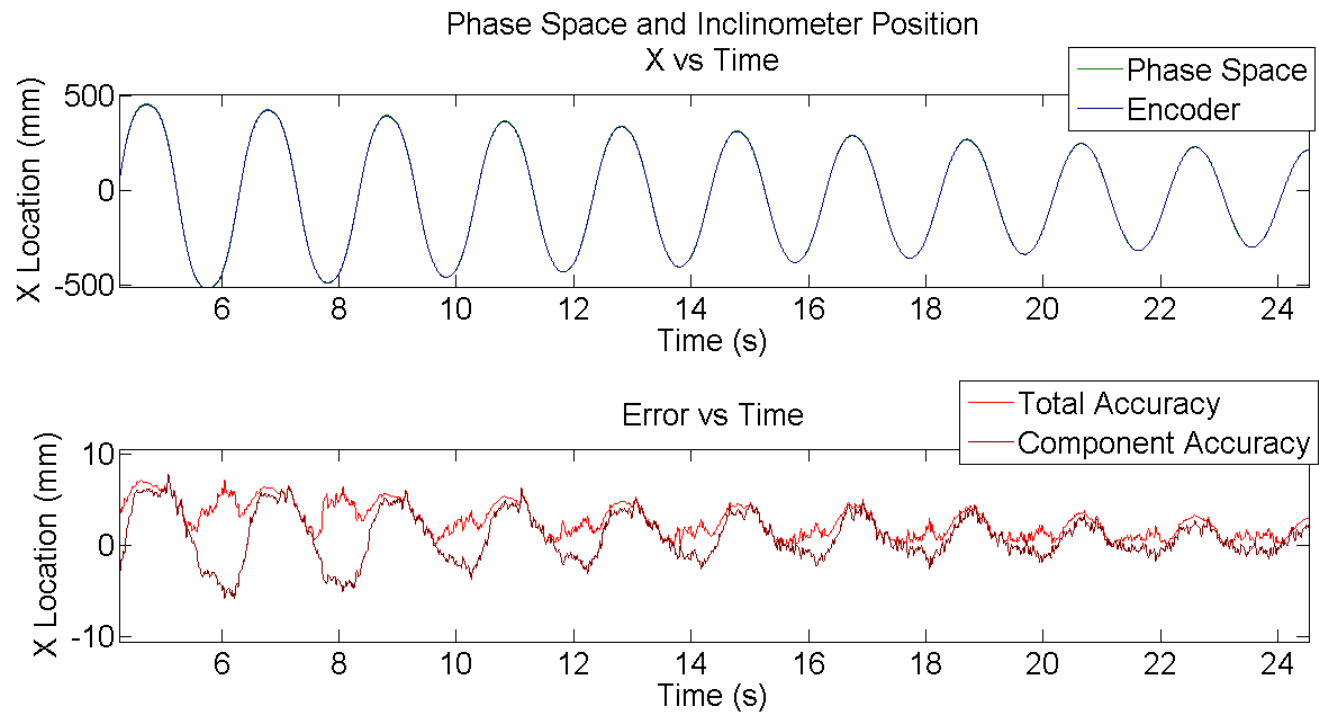


Figure 17: x position signals and accuracy vs. time.

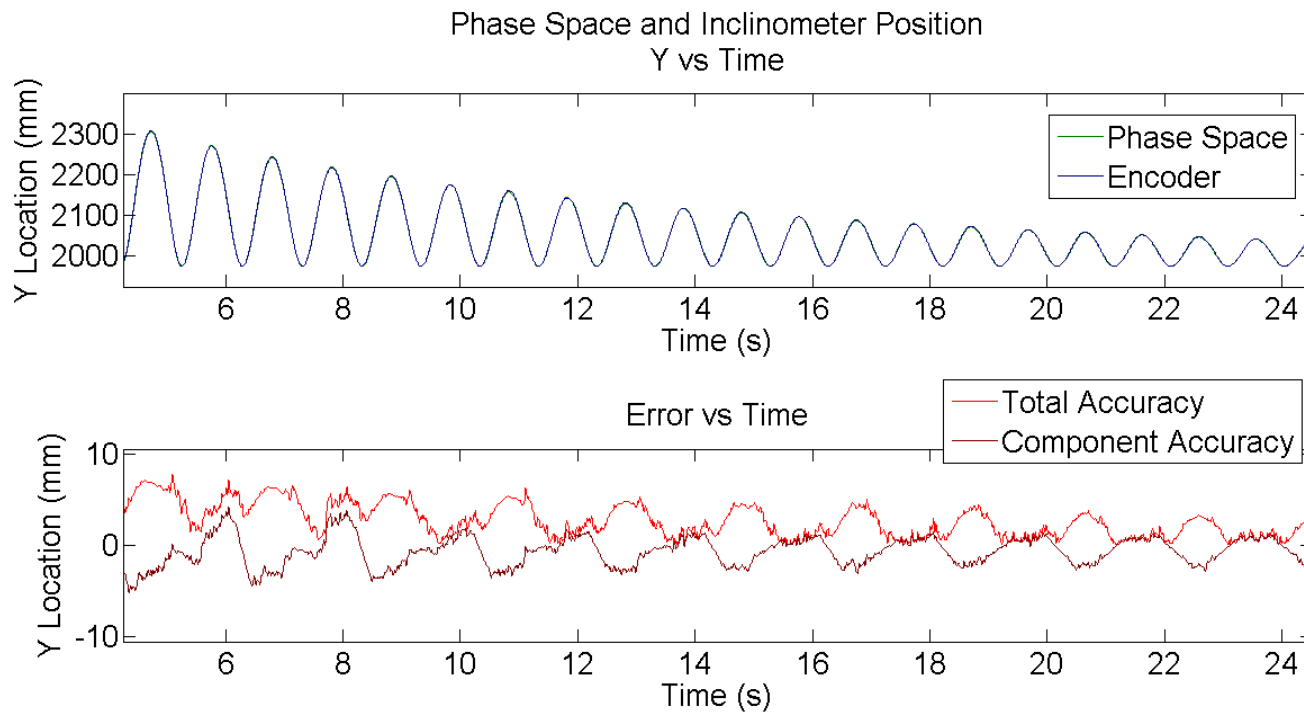


Figure 18: y position signals and accuracy vs. time.

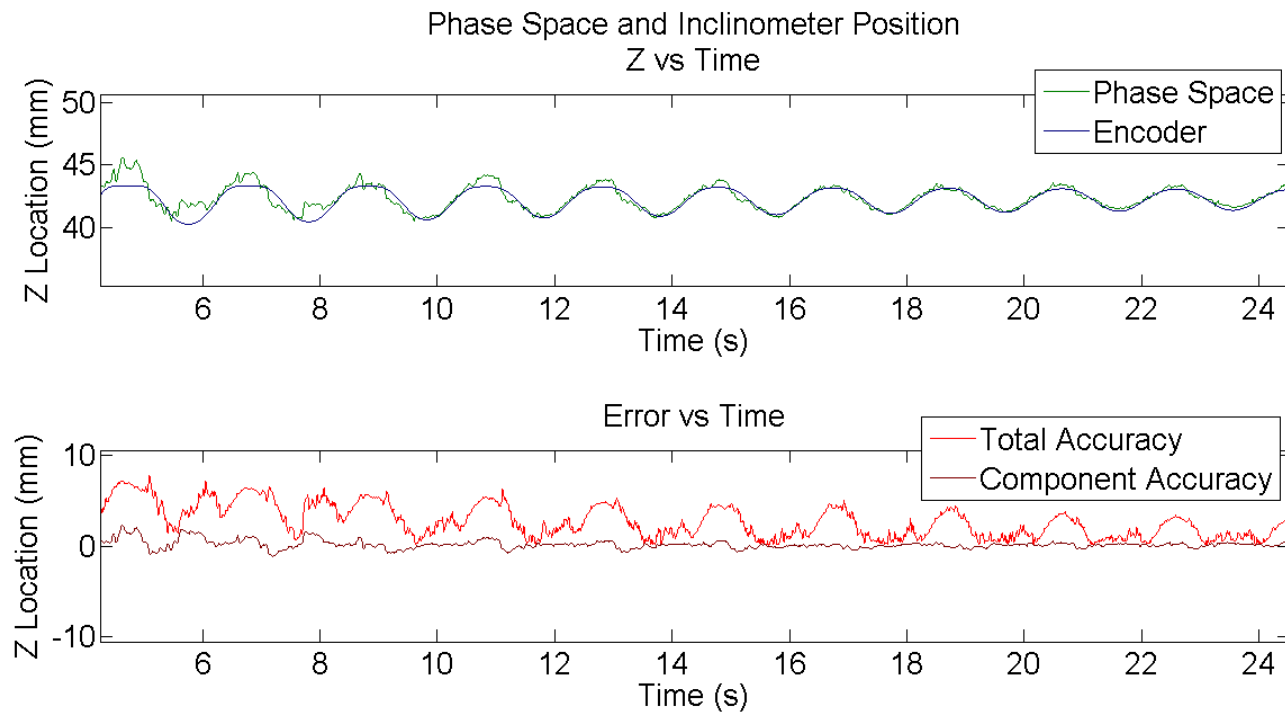


Figure 19: z position signals and accuracy vs. time

Table 2 shows the mean and standard deviation of the component x, y and z accuracies as well as the mean and standard deviation of the total signal for the first trial.

Table 2: Component and total signal accuracy and standard deviation, first trial.

	Accuracy Mean	Accuracy Standard Deviation
x Component	0.69 mm	2.58 mm
y Component	0.56 mm	1.55 mm
z Component	0.19 mm	0.47 mm
<b>Total Signal</b>	<b>2.56 mm</b>	<b>1.88 mm</b>

Table 2 shows that the average total error for the entire time series is 2.56 mm with a standard deviation of +/- 1.88mm. It also shows that a very small component of the total error is accounted for by the z component.

Velocity of the rigid body was calculated by taking the magnitude of the vector between two adjacent points in the time series and multiplying it by the frequency.

$$Velocity = \left( \sqrt{(x_i - x_{i-1})^2 + (y_i - y_{i-1})^2 + (z_i - z_{i-1})^2} \right) * frequency$$

Where i-1 and i mark two consecutive samples in the signal.

The calculated velocity error for the PhaseSpace signal was found by taking the difference between calculated velocity of the PhaseSpace signal and the optical encoder signal. Both of the velocity signals and the PhaseSpace error are shown in Figure 34

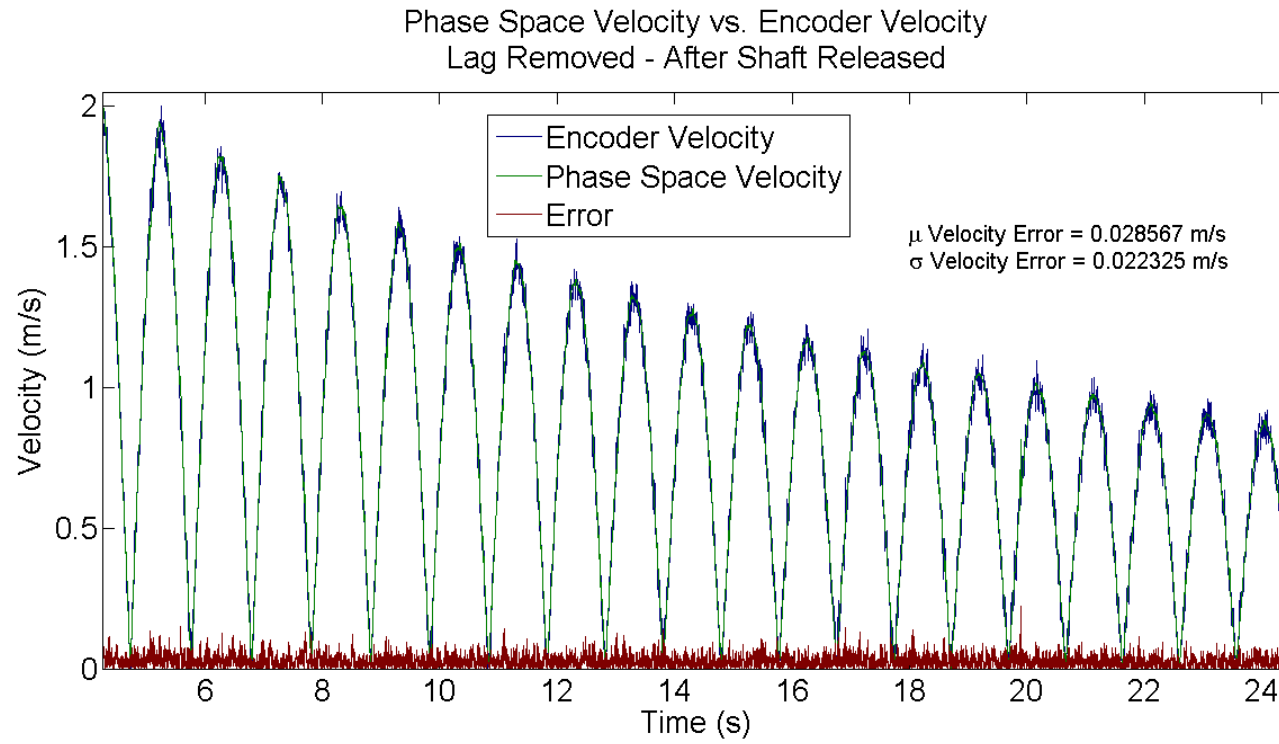


Figure 20: Calculated velocity and accuracy vs. time

The mean of the calculated velocity error for the time series is 0.029 m/s with a standard deviation of  $\pm 0.022$  m/s.

Figures 35 through 38 organize each PhaseSpace measurement into bins based on the respective velocity of each measurement. They present the mean and standard deviation of the accuracy of the position measurements in 21 0.1 m/s wide bins ranging from zero to 2.1 m/s. The mean is marked with an x and the range representing  $\pm$  one standard deviation is shown with an error bar.

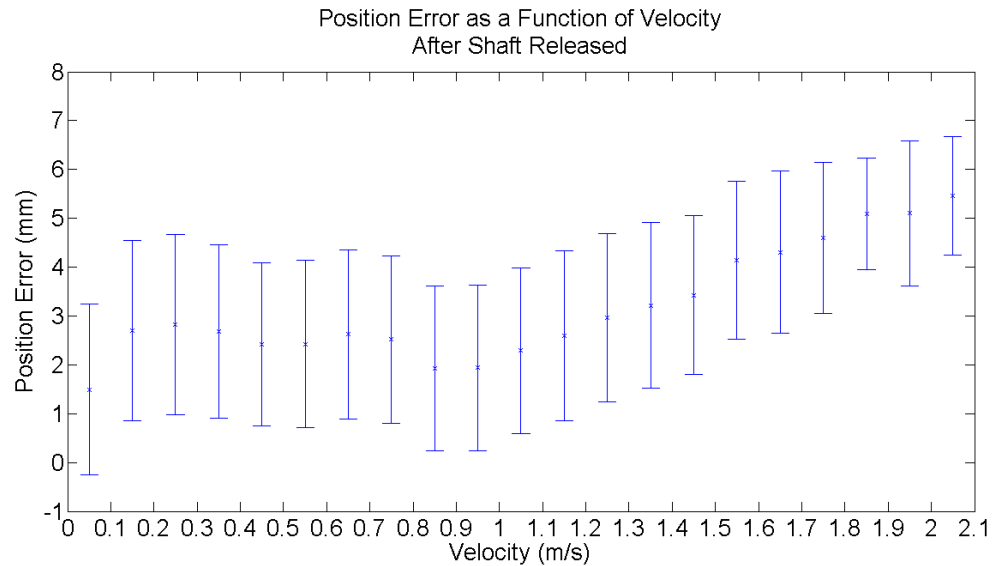


Figure 21: Position error as a function of velocity, first trial.

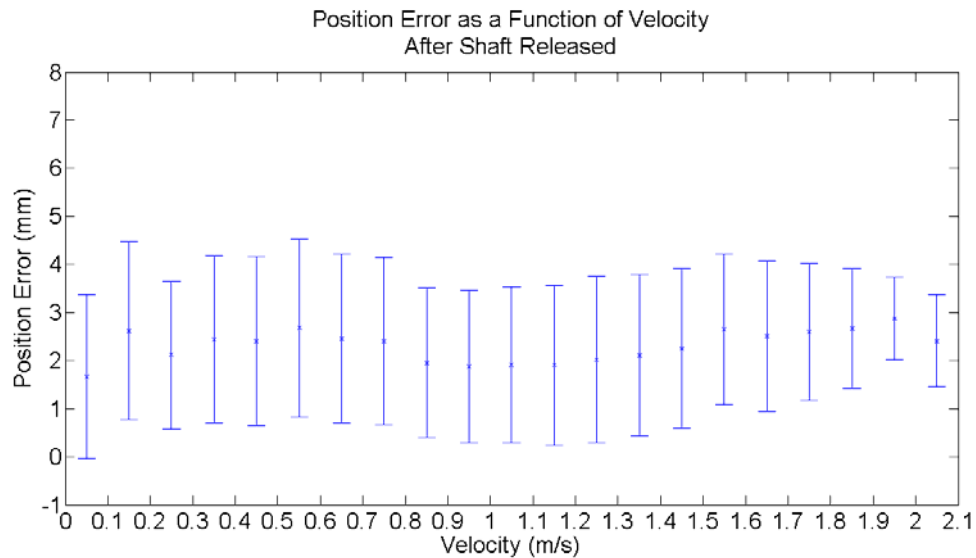


Figure 22: Position error as a function of velocity, second trial.

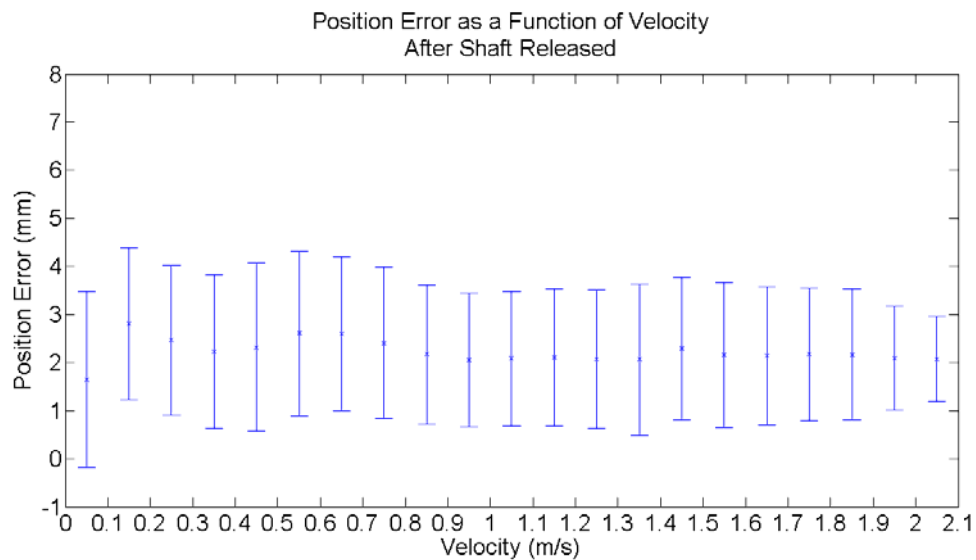


Figure 37: Position error as a function of velocity, third trial.

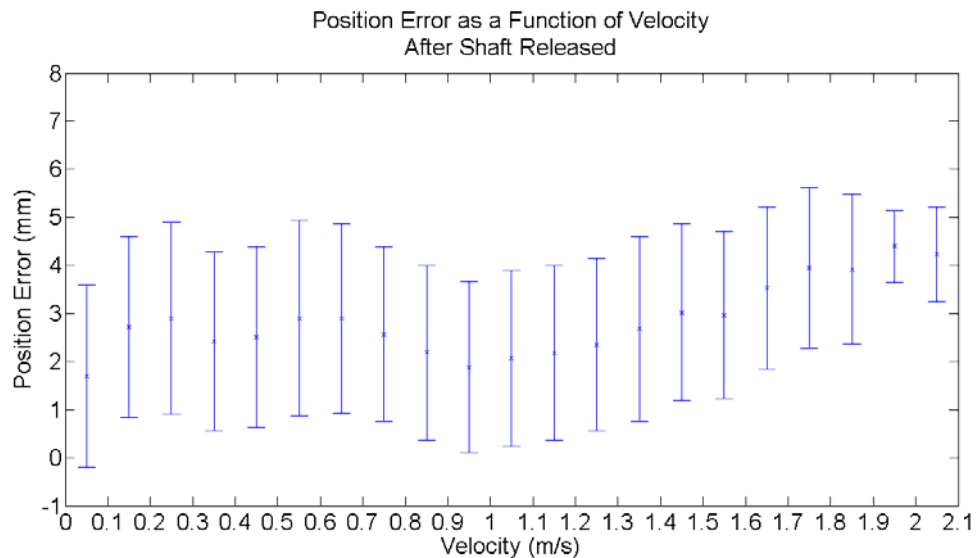


Figure 38: Position error as a function of velocity, forth trial.

To further investigate the relationship between accuracy and velocity, position error and time were plotted as functions of velocity in Figure 39 for the first trial. Error is represented by the vertical axis, velocity by the horizontal axis and time is represented with color.

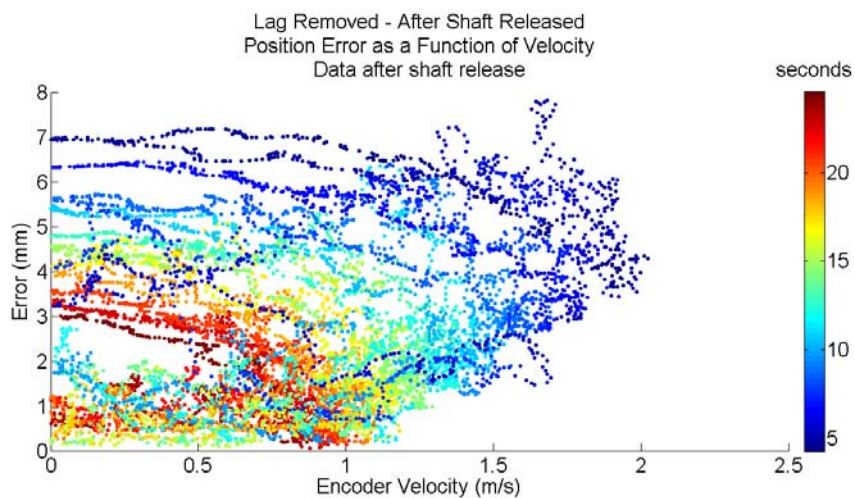


Figure 39: Accuracy and time as functions of velocity.

Figure 42 shows that error decreases with velocity, as well as time. As time goes on, the amplitude of the pendulum, both in the x and y directions, decreases. As it does accuracy increases.

Table 3 presents the mean and standard deviation of the error of the PhaseSpace signal for the three additional trials.

Table 3: PhaseSpace Error Mean and Standard Deviation for All Trials

	Mean Error	Standard Deviation
Trial One	2.25	1.66
Trial Two	2.17	1.7
Trial Three	2.22	1.59
Trial Four	2.48	1.93
<b>Mean</b>	<b>2.28</b>	<b>1.72</b>

## 5 Discussion

### 5.1 Static Test Discussion

During the static test the distance between two rigid bodies was recorded for 25 seconds at 480 Hz. The mean distance and the standard deviation of the distance was presented. This was repeated to provide samples at thirty locations throughout the measurement field.

#### *5.1.1 Accuracy and Precision Dependency on Location*

If the accuracy or precision of PhaseSpace measurements is dependent on the location the measurement is taken in the capture volume a trend should be noticed in the horizontal and vertical plane shown in Figures 24 through 27. The presence of a protective coat of epoxy, or the length of calibration, should not affect the trend. It was expected that the poorest accuracy and precision would be found at locations farthest from the aim point of the PhaseSpace cameras, at the limits of the cameras field of view.

This means that in Figures 24 through 27 the lowest measurements closest to the perimeter of the measurement field (lower right) should have the poorest precision and/or accuracy.

The accuracy plots show that accuracy tends to decrease as elevation increases. They also show that the poorest accuracy values are located near the perimeter. This pattern is roughly the same in each of the four conditions, though to varying extents. The magnitude of the poorest accuracies at the perimeter is approximately 0.5mm.

The most likely explanation for the pattern is that the operator collected less calibration data in the proximity of the poorer accuracy measurements than others. It is more difficult to collect calibration data at points over the operators head, and it is reasonable to assume that the operator developed a habit of neglecting certain areas during calibration. Indeed, close inspection of Figure 5 shows that some areas of the measurement field contained a lower calibration data density than others.

The precision plots in Figures 24 through 27 do not show a trend indicating that precision varies significantly as a function of location. Only in Figure 26 does a trend appear to exist with poorer precision in the lower center and upper perimeter of the field. However, Figures 24, 25 and 27 do not support this observation.

### *5.1.2 Accuracy and Precision Dependency on the Length of Calibration*

During the analysis of the effect of location in the measurement field it was shown that the density of calibration may affect accuracy. This means that the longer calibration length which includes more calibration data should be more accurate than the shorter calibration length.

Table 1 shows that for the epoxy encased LEDs the eight minute calibration was less accurate than the four minute calibration. The values of standard deviation show that the eight minute calibration also had more variation than the four minute calibration. Therefore, the epoxy encased LED data shows that calibration length negatively effects accuracy. This was not expected.

The exposed LEDs show the opposite trend. The longer calibration length proved to be more accurate than the shorter calibration length. If calibration has an effect on accuracy, both sets of LEDs would show the same trend. The fact that opposite trends exist between LED types shows that this test cannot link calibration length to accuracy.

Similar arguments show that the eight minute calibration proved to be more precise than the four minute calibration for both LED types. It can also be shown that the variation of the measurements increased for the longer calibration. Therefore, this experiment shows that precision may improve with calibration length, but that a wider range of precisions may become possible.

### *5.1.3 Accuracy and Precision Dependency on Epoxy Encapsulation*

Table 1 shows that for the eight minute calibration the exposed LEDs were more accurate and precise than the epoxy LEDs. Accuracy and precision appear to be negatively impacted by epoxy encapsulation. However, it is shown that the effect is slight. The difference between the mean accuracy measurements is 0.16 mm and the difference between the mean precision measurements is 0.33 mm.

The four minute calibration is vastly different. In this case the epoxy LEDs were more accurate by 0.64 mm, though the exposed LEDs were more precise by 0.5 mm.

For both calibrations, the variation of accuracy and precision was greater for the epoxy LEDs than the exposed LEDs.

## 5.2 Dynamic Test Discussion

The accuracy of the PhaseSpace system determined by the dynamic test varied in each of the four trials. The mean accuracy varied from of 2.17 mm to 2.48 mm while the standard deviation varied from 1.59 mm to 1.93 mm. The mean accuracy and standard deviation of all trials combined was  $2.28 \pm 1.72$  mm.

### 5.2.1 Error in the Encoder Signal

Figures 43 and 44 show closer views of the PhaseSpace signal in the x direction for the first and last peaks of the first trial. They show that most of the error associated with the PhaseSpace signal happens at the peaks, where velocity is low. This error reduces with the amplitude of the signal. Also plotted in Figures 40 and 41 is the error that could be present in the encoder signal from the measurements of  $l$  and  $w$  and the possible error of the optical encoder. The PhaseSpace signal is plotted in green, the encoder signal in blue and the ranges of possible error are plotted in dashed blue lines. The PhaseSpace error signal is always outside of the bounds of the encoder error, except for locations where the PhaseSpace signal crosses the encoder signal. This validates the use of the encoder signal as a standard to compare with the PhaseSpace signal for accuracy determination.

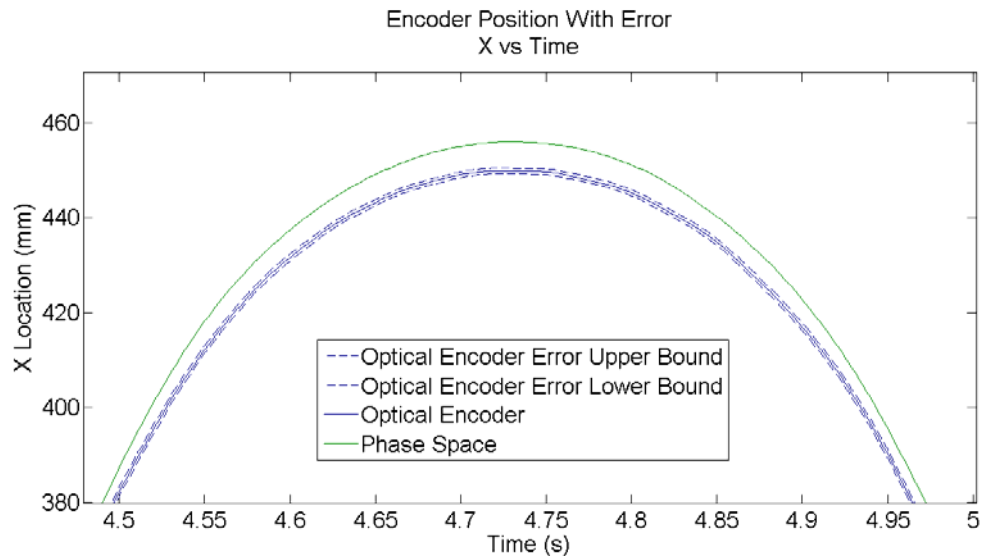


Figure 23: Encoder error vs PhaseSpace error; x signal, first peak.

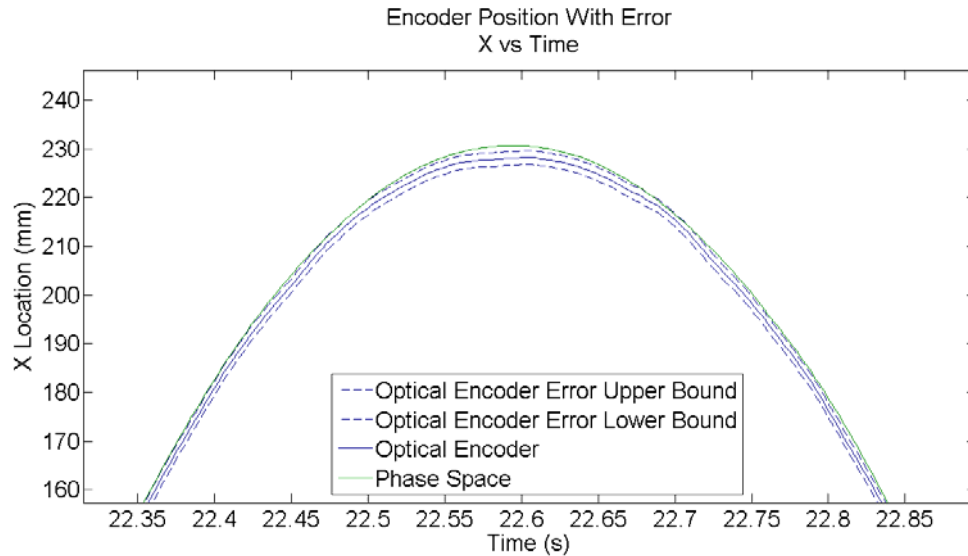


Figure 24: Encoder error vs. PhaseSpace error; x signal, last peak.

### 5.2.2 Pendulum Movement Outside of $x''-y''$ Plane

Movement of the pendulum that was outside of the  $x''-y''$  plane resulting from flex in the pendulum shaft or slop in the box bearings was not recorded by the optical encoder. However, this movement, or "wobble" can be seen in the PhaseSpace signal. Figure 45 shows the z component of the PhaseSpace signal for the first trial after the signal has been rotated so that its new x-y plane is parallel with the  $x''-y''$  plane of the encoder and its x-z plane is parallel with the pendulum axle. Also included is the total error calculated for the PhaseSpace signal. Figure 42 shows that the error resulting from not including the "wobble" is small and could be disregarded.

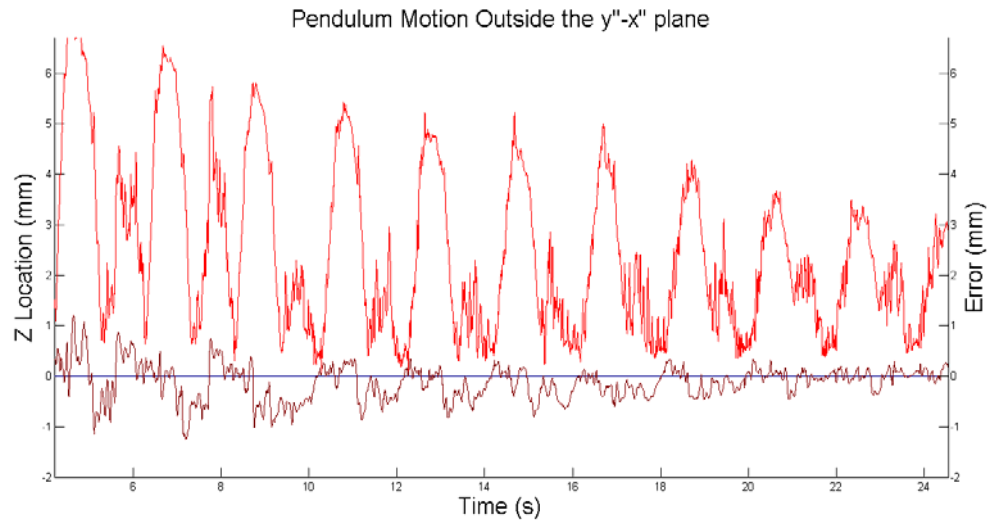


Figure 25: Pendulum Motion Outside of  $x'$ - $y'$  plane.

### 5.2.3 Accuracy and Precision Dependency on Velocity

In Figure 38 the mean accuracy appears to stay constant at about 2.5 mm until velocity reaches one meter per second, at which point it increases linearly to 5.5 mm at over two meters per second. Error bars representing precision also appear to decrease at the higher velocities. Therefore, with increasing velocity accuracy appears to decrease but precision becomes greater.

Figures 39 through 41 show similar plots for the additional trials of the dynamic test. They show that the trend described above was not repeatable; accuracy does not always decrease with velocity. However, in each figure the greatest precision, (smallest error bars), was seen at the highest velocities. Precision increases with velocity.

### 5.2.4 Accuracy Dependency on Pendulum Amplitude

The cause of the relationship between error in the PhaseSpace signal and the amplitude of pendulum motion is not certain. The accuracy of the LED position measurements was examined as a possible source of error that may cause this phenomenon. A computer script was written to iteratively change the measurements and

determine which values of  $l$  and  $w$  provide the best possible accuracy. However, using this "best possible" geometry, an accuracy dependency on amplitude was still observed.

Another cause for the amplitude-error relationship could be that the location in space where the peak amplitudes occurred may not have as much calibration data as the location of the rest position. During the static discussion it was proposed that calibration density may be linked to error. If this is true, and the operator collected more data at the rest position of the pendulum then the areas where the pendulum reached its maximum  $x''$  and  $y''$  amplitudes, then we would expect to see the observed relationship between amplitude and accuracy.

A final plausible explanation may be there is movement or flex in the axle, the shaft or in the adhesion of the LEDs to the shaft. Larger shaft rotations and their greater velocities and forces would amplify any sort of movement or flex, increasing error.

## **6 Conclusion**

### 6.1 Static Accuracy and Precision

#### *6.1.1 Location in the Measurement Field*

Figures 24 through 27 show that there is a trend in the distribution of accuracy throughout the measurement field. It is shown that accuracy tends to decrease as elevation increases. It is also shown that accuracy is more poor near the perimeter, as expected. The magnitude of the error at the perimeter of the measurement field is approximately 0.5mm. The poor accuracy at higher elevations (closer to the aim-point of the cameras) was unexpected. The most likely explanation for this pattern is that accuracy depends on the density of calibration data and the operator failed to collect sufficient data in the proximity of the higher elevations. Precision was found to not vary throughout the measurement field.

### *6.1.2 Calibration Length*

Data collected from epoxy encased LEDs showed that calibration length negatively affected accuracy. Data collected from exposed LEDs showed the opposite, that calibration length positively effects accuracy. Therefore, no reasonable conclusion can be made for the affect of calibration length on accuracy. Precision was shown to be greater after an eight minute calibration than after a four minute calibration.

### *6.1.3 Epoxy Encapsulation*

Information from Table 1 was shows that the mean accuracy and precision with an eight minute calibration decreased with epoxy encapsulation by 0.16 mm and 0.33 mm respectively. Data from the four minute calibration shows that the mean accuracy increased with epoxy encapsulation by 0.64 mm and mean precision decreased by 0.5 mm. The reason for the discrepancy between the two calibrations is unknown. Because the eight minute and four minute calibrations do not show a consistent effect of epoxy encapsulation, this test failed to show any relationship between accuracy and epoxy encapsulation. Precision was shown to decrease by as much as 0.5 mm.

### *6.1.4 Accuracy and Precision Under Wave Lab Conditions*

Current PhaseSpace experimentation in the Hinsdale Wave Lab uses the epoxy encased LEDs. Table 1 shows that the eight minute calibration for the epoxy encased LEDs provided less accuracy than the four minute calibration for epoxy encased LEDs. Therefore, a conservative evaluation of the accuracy of the epoxy encased LEDs would use the data from the eight minute calibration. Also, in practice in the Hinsdale Wave Lab calibrations as short as four minutes are rare. The fact that an operator is usually wading through water and around instruments means that more time is required to cover

all of the measurement field. Therefore, it is best to use the eight minute calibration data to determine the accuracy and precision of the epoxy LEDs. The mean accuracy of all of the measurements in the measurement field was found to be 2.11 mm and vary with a standard deviation of 1.97 mm. The mean precision (a 97% confidence interval) was found to be 0.94 mm and vary with a standard deviation of 0.56 mm.

Assuming that the PhaseSpace system provides location information with accuracy and precision that are normally distributed; and considering the limit of the mean plus two standard deviations; it can be shown that phase space can be expected to record the distance between two rigid bodies with an accuracy of at least 6.05 mm and precision of at least 2.06 mm. To find the accuracy and precision for a single rigid body these values are divided by two. Therefore, with epoxy LEDs and an eight minute calibration, it is reasonable to assume that the accuracy and precision for a single, static rigid body measured by the PhaseSpace system is at least 3.0 mm and 1.0 mm, respectively.

## 6.2 Dynamic Accuracy

In the dynamic test the mean accuracy for all trials was found to be 2.28 mm with a standard deviation of 1.72 mm. Velocities oscillated from zero to 2.1 meters per second during the experiment. Figure 42 shows that accuracy is dependent upon the amplitude of the pendulum swing. Possible reasons for this could include the density of calibration data, or, flex in the pendulum shaft, movement of the pendulum axle, movement in the box bearings or movement of the LEDs themselves at higher velocities. Finally, Figures 38 through 41 do not show a consistent relationship between velocity and accuracy.

### 6.3 Future Work

Questions remain about the effect of calibration and epoxy encapsulation on accuracy. It was shown, but not proven, that the density of calibration data *may* cause changes in accuracy throughout the measurement field. The static test has shown that the accuracy of epoxy encased LEDs increased with calibration time while the accuracy of exposed LEDs decreased with calibration time. This suggests that accuracy can vary widely between calibrations of the same length. Similar conclusions can be reached by evaluating the effect of epoxy encapsulation. Additional experiments should compare accuracy data over a wider range of calibration times, taking steps to ensure that calibration data is evenly spread, with multiple trials of each calibration time. Multiple trials at each calibration time will help to ensure that the true mean accuracy for a given calibration length is understood. Examining more different calibration lengths could link calibration length to accuracy and definitively show a trend of increasing precision with increasing calibration time.

The pendulum/optical encoder assembly was not a perfect system to provide "known" movement to compare the PhaseSpace signal with. While steps were taken to minimize it, error existed in the form of bending of the aluminum shaft, slop in the axle and bearings or movement from weak LED to shaft adhesion. The need to make two additional length measurements in addition to a single angle measurement from the optical encoder also increased the possibility of error.

Future experiments might consider a different ways to create known motion. Systems that would allow velocity to remain constant during the experiment would allow more information to be collected at a specific velocities of interest.

## 6.4 Final Conclusions

The combined accuracy found for all dynamic test trials of  $2.28 \text{ mm} \pm 1.72 \text{ mm}$  is reasonably close to the  $1.06 \pm 0.98 \text{ mm}$  result found for the epoxy encased LEDs during the static test. The combination of the static and dynamic tests show that the PhaseSpace measurement system can provide position measurements within 5.7 mm of their real value, regardless of location in the measurement field, calibration length, or velocity. Precision (97% confidence interval) for a single, static rigid body was found to be 0.8 mm. Precision may increase with calibration time, increases with velocity but is not effected by location in the measurement field. The effect of epoxy encapsulation on accuracy and precision was shown to be on the order of tenths of millimeters.

## **Bibliography**

Castro et al. 2005. Design and evaluation of a new three-dimensional motion capture system based on video. *Gait and Posture* 24, 126-129.

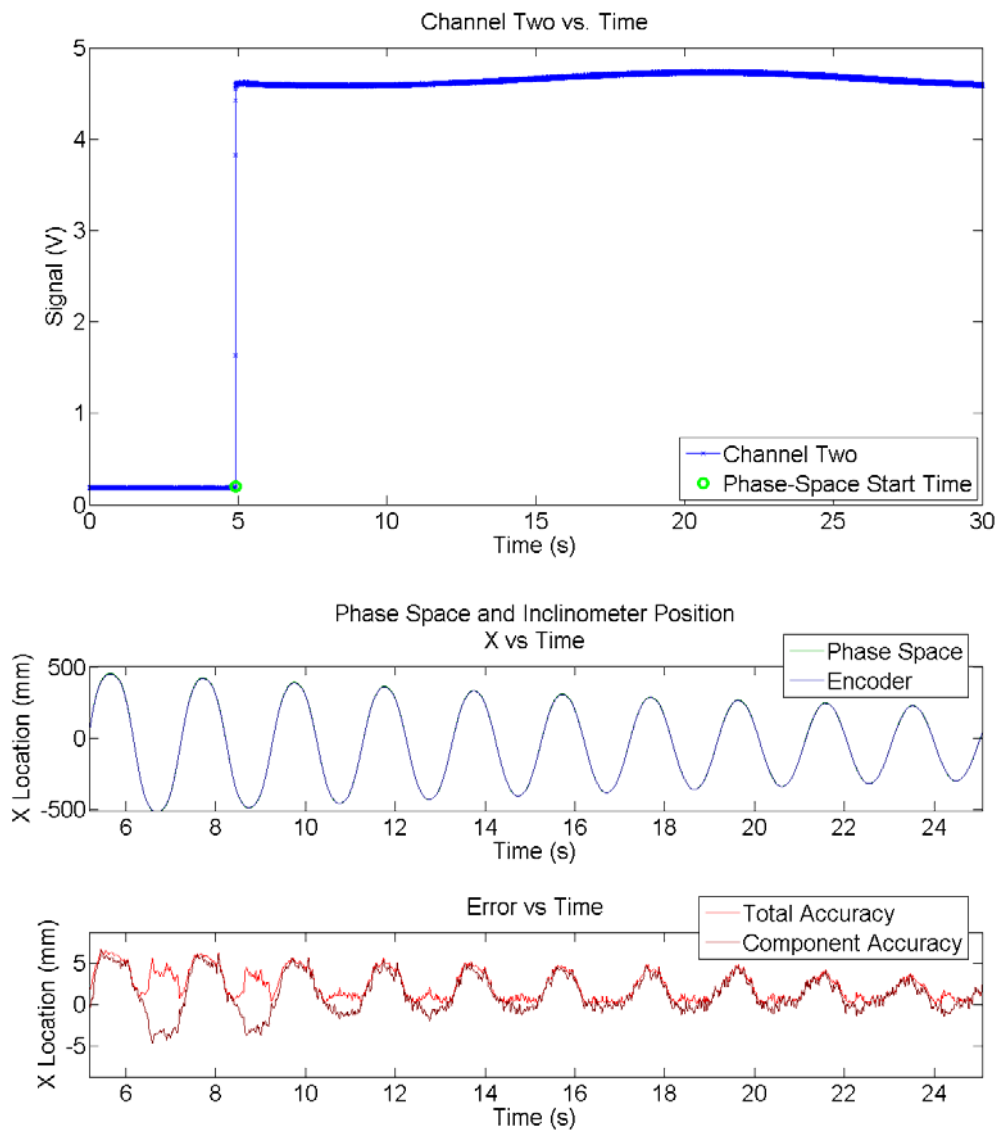
DeLuzio et al. 1993. A procedure to validate three-dimensional motion assessment systems. *Journal of Biomechanics* 26, no. 6: 753-759.

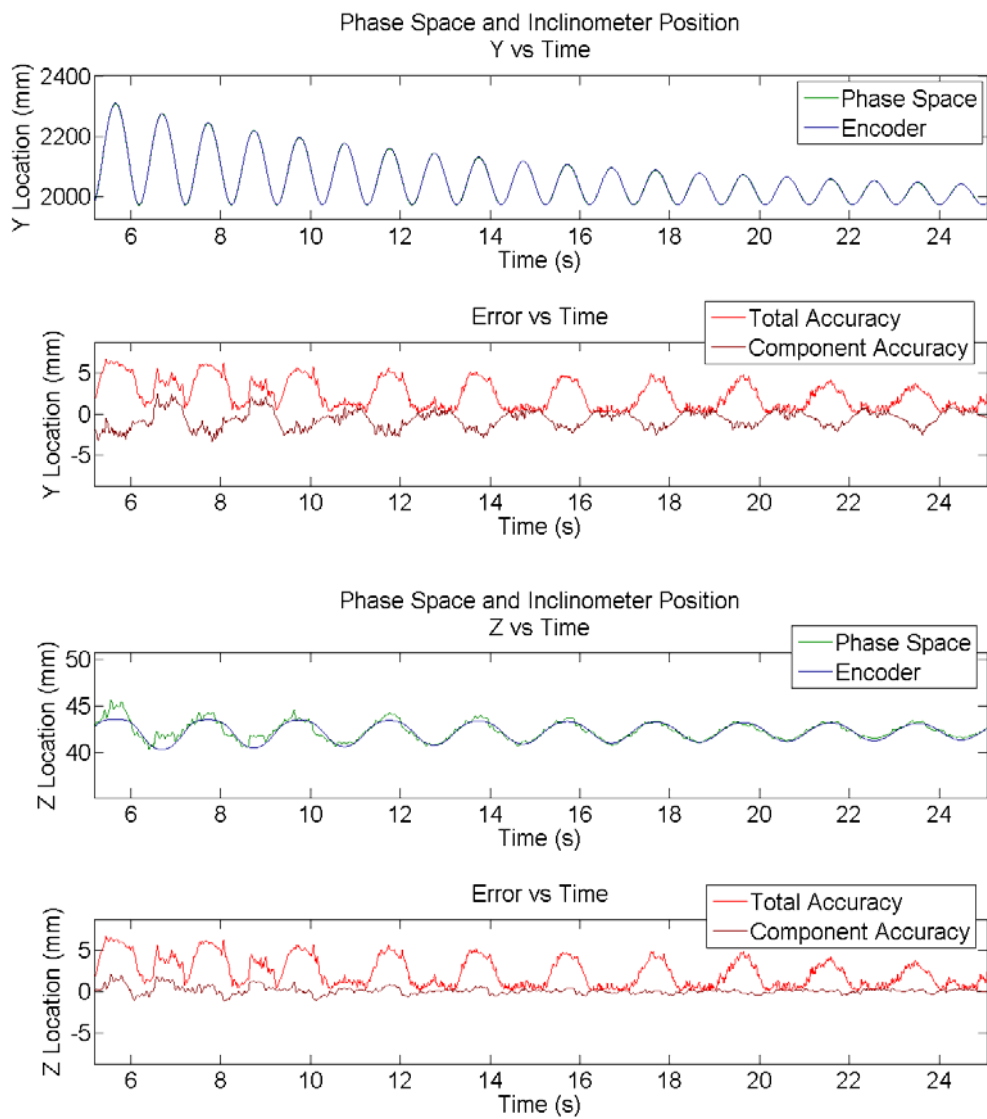
Rhinefrank et al. 2010. High resolution wave tank testing of scaled wave energy devices. Paper presented at the 29<sup>th</sup> International Conference on Offshore Mechanics and Arctic Engineering.

Teeple et al. 2009. Pendulum-based method for determining the temporal accuracy of digital video-based motion capture systems. *Gait & Posture* 29: 349-353.

## **Appendices**

## Appendix A: Trial Two Figures





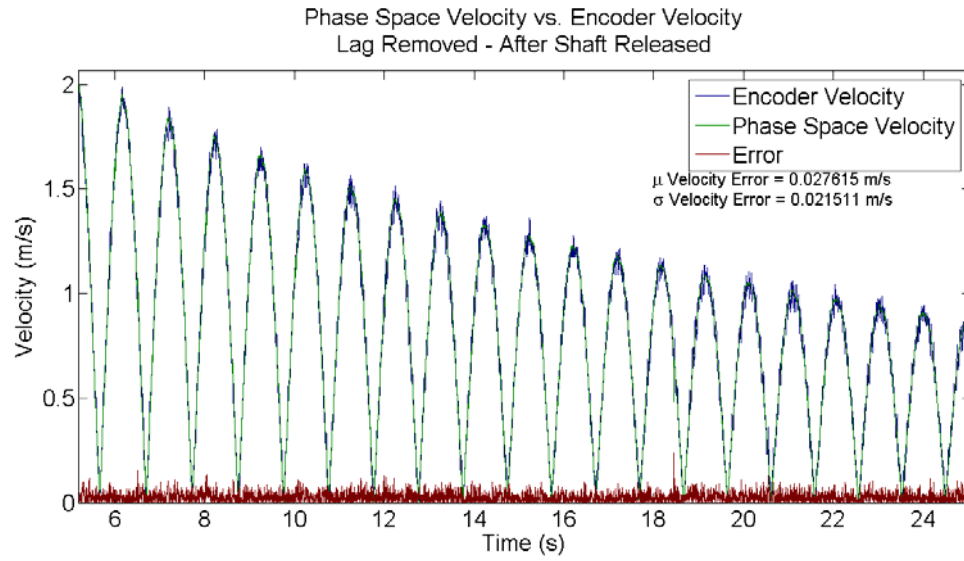
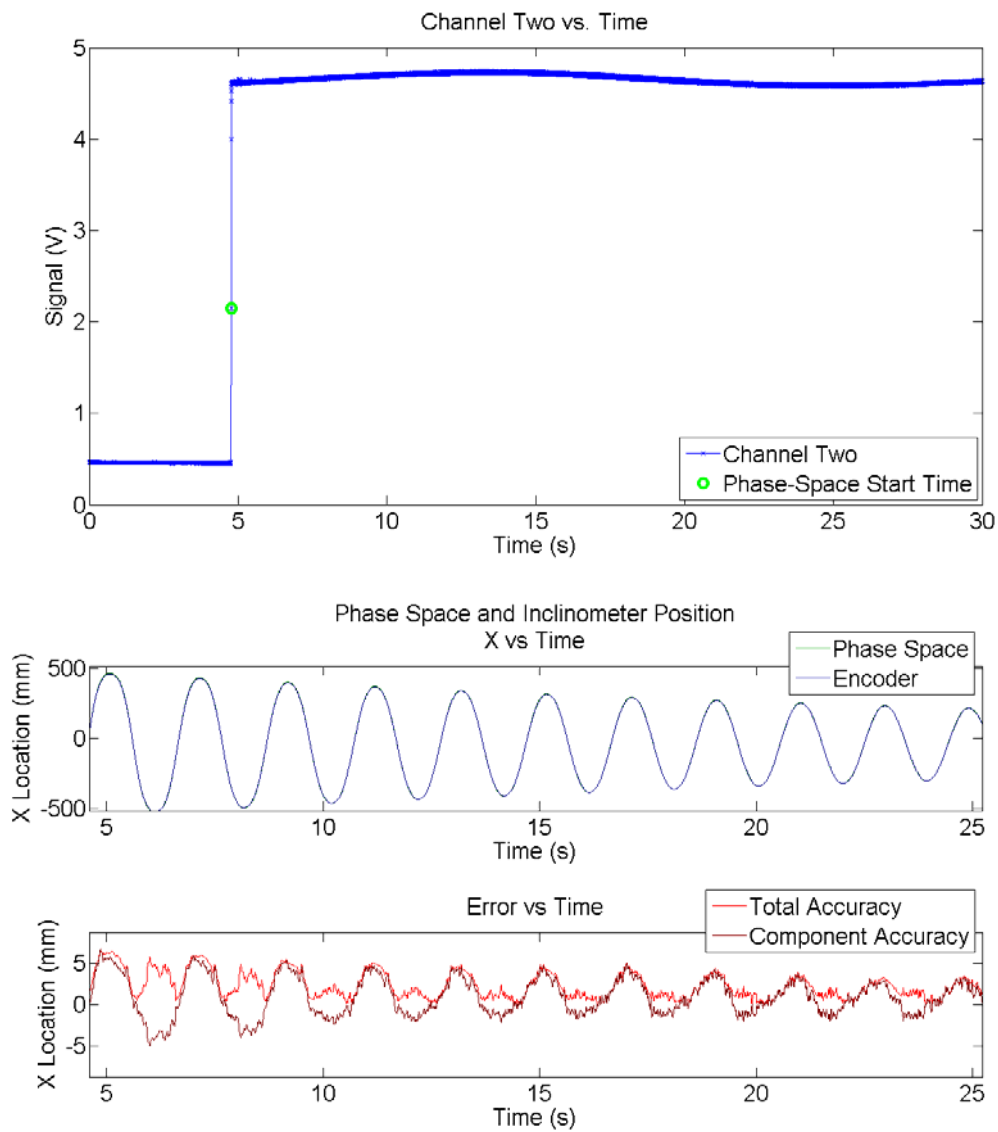
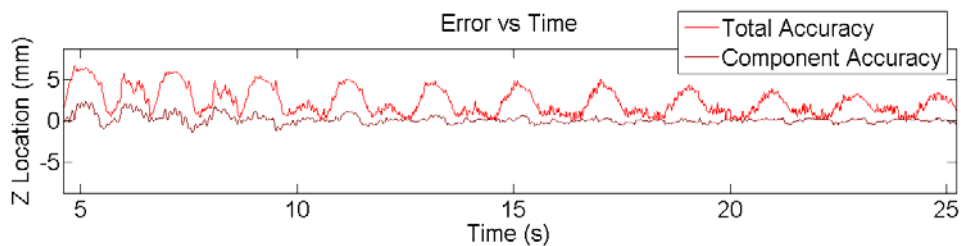
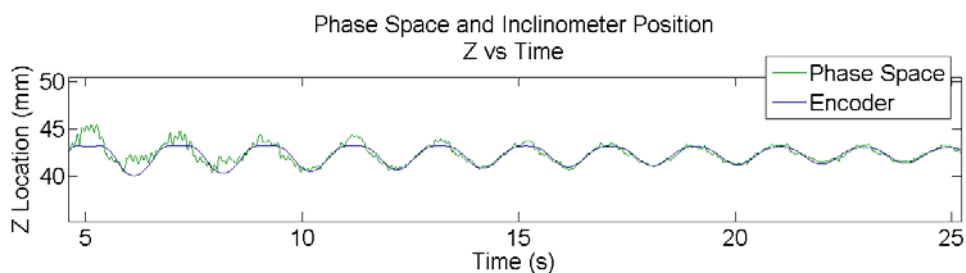
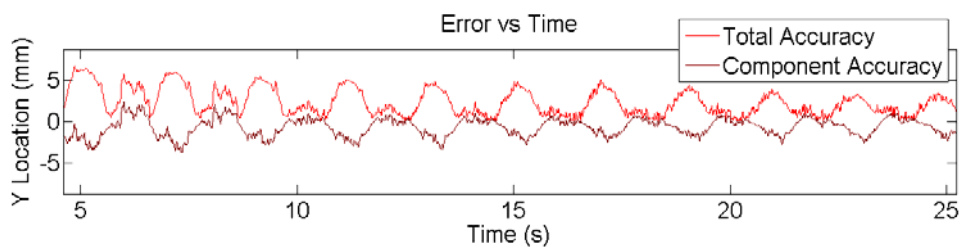
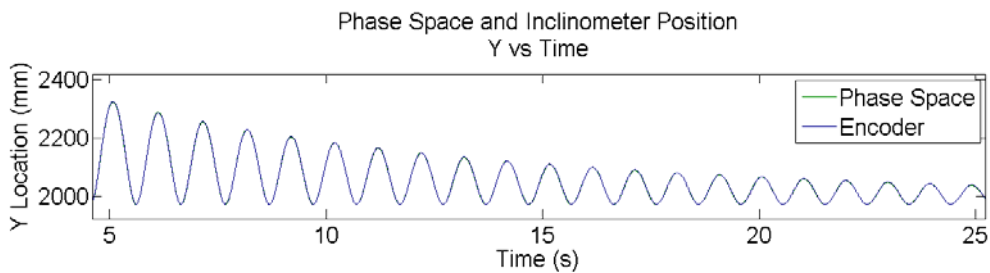


Table 4: Component and Total Signal Accuracy and Standard Deviation, Second Trial

	Accuracy Mean	Accuracy Standard Deviation
x Component	0.91 mm	2.28 mm
y Component	0.62 mm	1.00 mm
z Component	0.14 mm	0.42 mm
<b>Total Signal</b>	<b>2.17 mm</b>	<b>1.70 mm</b>

## Appendix B: Trial Three Figures





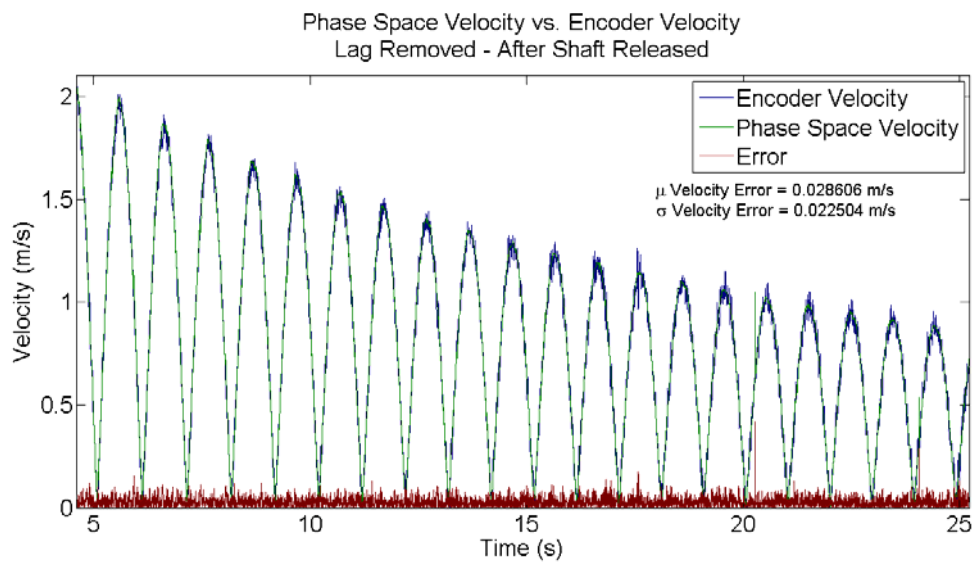
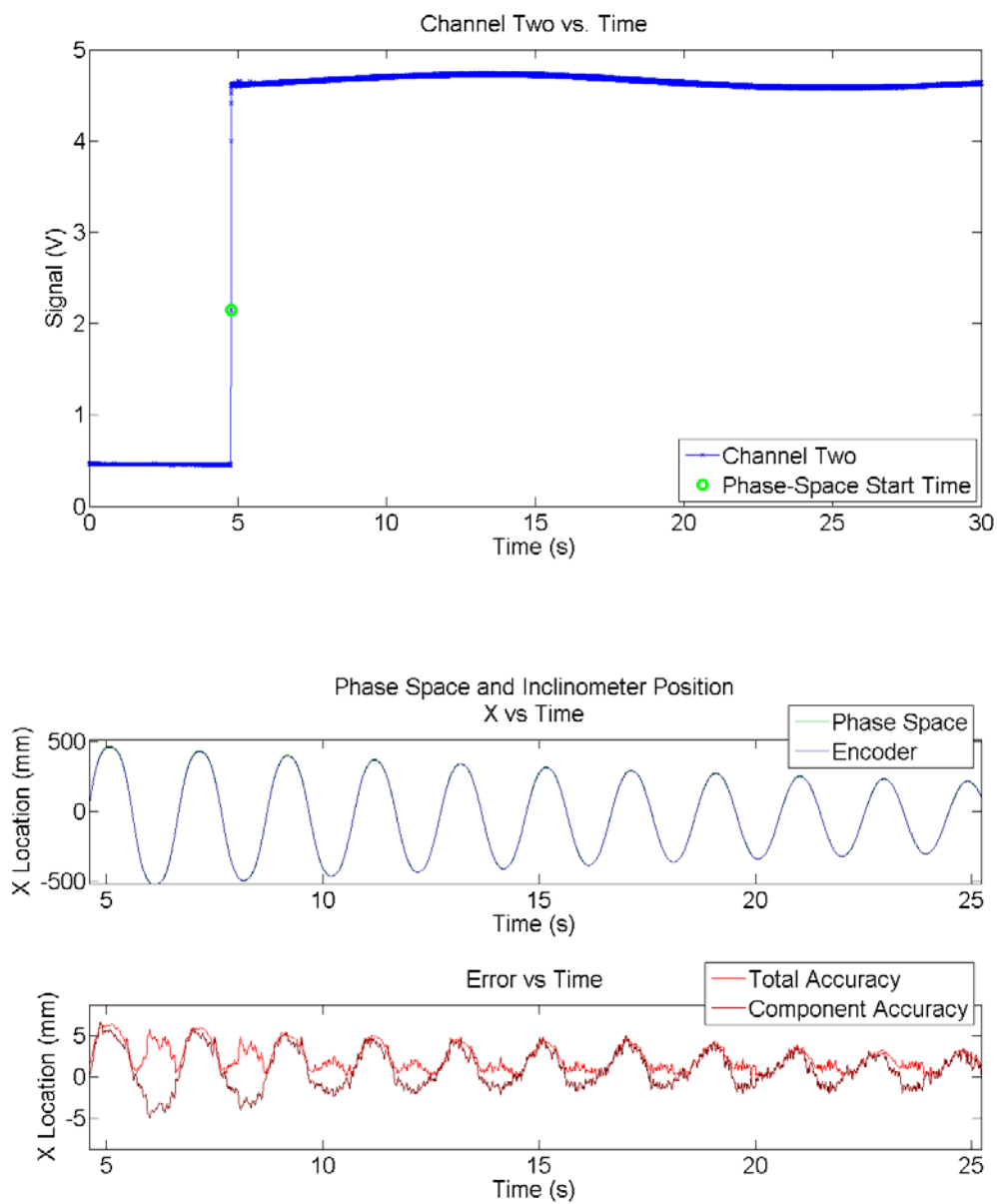
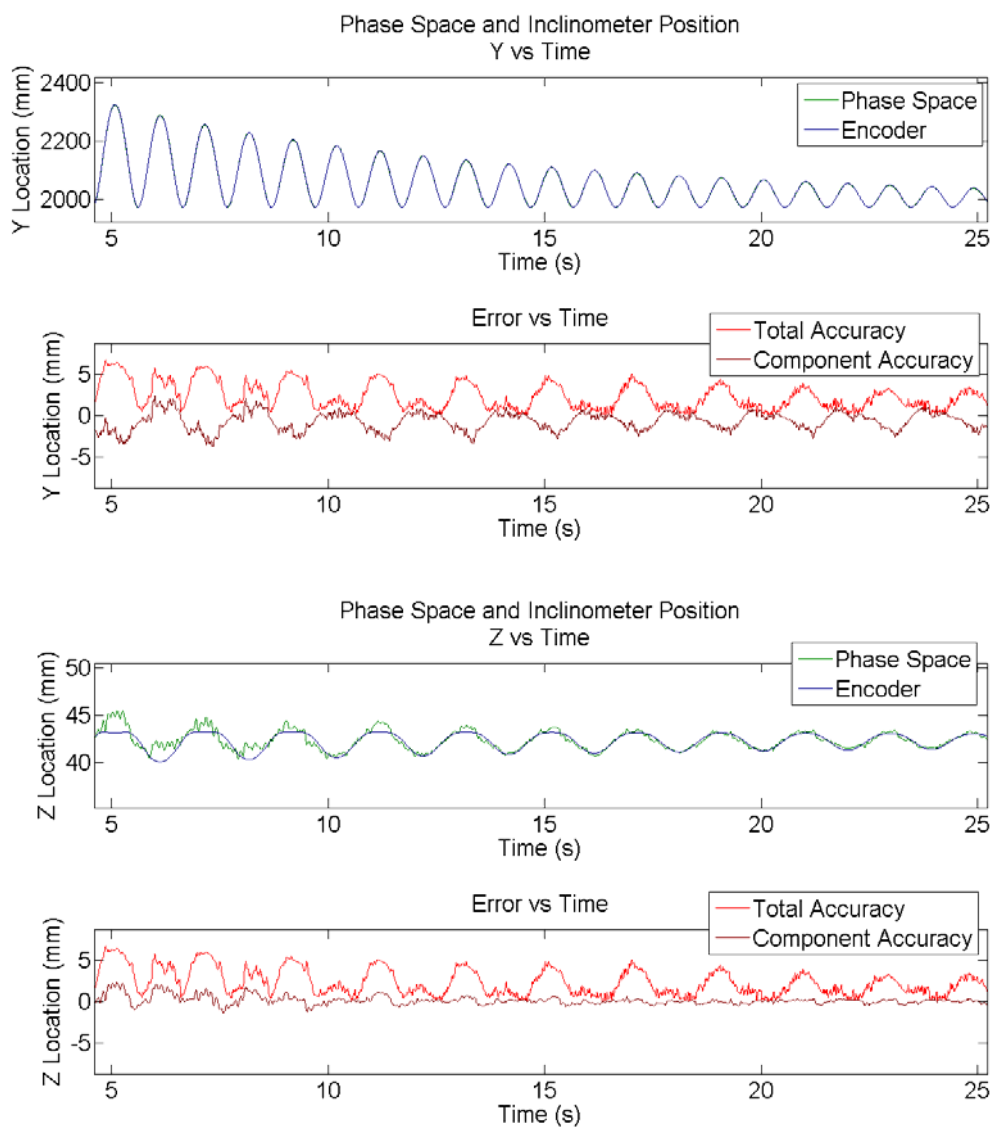


Table 5: Component and Total Signal Accuracy and Standard Deviation, Third Trial

	Accuracy Mean	Accuracy Standard Deviation
x Component	0.64 mm	2.29 mm
y Component	0.61 mm	1.02 mm
z Component	0.22 mm	0.59 mm
<b>Total Signal</b>	<b>2.22</b>	<b>1.59</b>

## Appendix C: Trial Four Figures





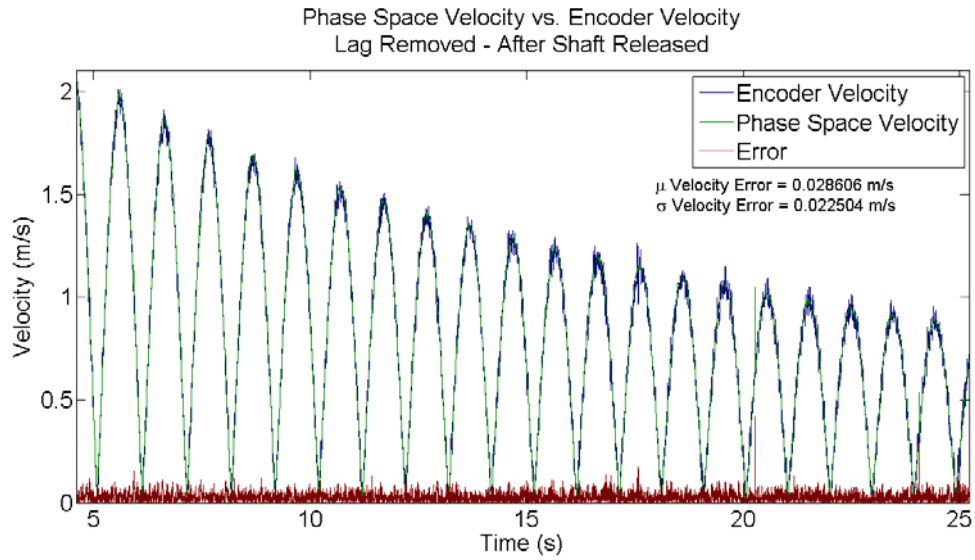


Table 6: Component and Total Signal Accuracy and Standard Deviation, Third Trial

	Accuracy Mean	Accuracy Standard Deviation
x Component	0.84 mm	2.45 mm
y Component	0.55 mm	1.53 mm
z Component	0.35 mm	0.65 mm
<b>Total Signal</b>	<b>2.48 mm</b>	<b>1.93 mm</b>